ENTRAINMENT OF A THERMAL WITH OR WITHOUT BUOYANCY REVERSAL IMPINGING ON A STRATIFIED INTERFACE

BY

QING ZHANG

A Thesis
Submitted to the Faculty of Graduate Studies in Partial
Fulfillment of the Requirements for the Degree of

MASTER OF SCIENCE

Department of Mechanical and Industrial Engineering
University of Manitoba
Winnipeg, Manitoba

© March, 1999

National Library of Canada
Acquisitions and Bibliographic Services
395 Wellington Street
Ottawa ON K1A 0N4
Canada

Bibliothèque nationale du Canada
Acquisitions et services bibliographiques
395, rue Wellington
Ottawa ON K1A 0N4
Canada

Your file Votre référence

Our file Notre référence

The author has granted a non-exclusive licence allowing the National Library of Canada to reproduce, loan, distribute or sell copies of this thesis in microform, paper or electronic formats.

L'auteur a accordé une licence non exclusive permettant à la Bibliothèque nationale du Canada de reproduire, prêter, distribuer ou vendre des copies de cette thèse sous la forme de microfiche/film, de reproduction sur papier ou sur format électronique.

The author retains ownership of the copyright in this thesis. Neither the thesis nor substantial extracts from it may be printed or otherwise reproduced without the author's permission.

L'auteur conserve la propriété du droit d'auteur qui protège cette thèse. Ni la thèse ni des extraits substantiels de celle-ci ne doivent être imprimés ou autrement reproduits sans son autorisation.

0-612-41651-8

Canada

THE UNIVERSITY OF MANITOBA

FACULTY OF GRADUATE STUDIES

*****

COPYRIGHT PERMISSION PAGE

ENTRAINMENT OF A THERMAL WITH OR WITHOUT BUOYANCY REVERSAL IMPINGING ON A STRATIFIED INTERFACE

BY

QING ZHANG

A Thesis/Practicum submitted to the Faculty of Graduate Studies of The University of Manitoba in partial fulfillment of the requirements of the degree

of

MASTER OF SCIENCE

QING ZHANG ©1999

Permission has been granted to the Library of The University of Manitoba to lend or sell copies of this thesis/practicum, to the National Library of Canada to microfilm this thesis and to lend or sell copies of the film, and to Dissertations Abstracts International to publish an abstract of this thesis/practicum.

The author reserves other publication rights, and neither this thesis/practicum nor extensive extracts from it may be printed or otherwise reproduced without the author's written permission.

University of Manitoba

Abstract

Laboratory experiments of a thermal with and without buoyancy reversal impinging on a stratified interface are presented. A thermal is created by releasing a small volume of buoyant fluid into a stratified environment composed of two layers of different densities. A thin interface separates the lower layer from the lighter upper layer. The entrainment of upper layer fluid into the thermal is investigated using a passive dye flow visualization technique. For the case of thermals without buoyancy reversal, the entrainment rate is found to obey a $Ri^{-3/2}$ power law, similar to the results obtained for stirring grid turbulence (Turner 1973) and a vertical plume impinging on a stratified interface (Kumagai 1984). This result was predicted by the stratified entrainment model of Cotel and Breidenthal (1997), using the concept of vortex persistence.

The effect of simulated evaporative cooling on the entrainment of a thermal impinging on a stratified interface is also investigated experimentally. Evaporative cooling in atmospheric clouds is simulated by buoyancy reversal in the laboratory, where the mixed fluid is denser than either parent parcel. This is realized in the laboratory by releasing a mixture of ethyl alcohol and ethylene glycol in an aqueous solution. It rises first through a relatively dense lower layer fluid and then impinges on a thin stratified interface, above which is a layer of relatively light fluid. The entrainment of upper layer fluid across the interface is measured optically. The entrainment rate for values of the buoyancy reversal parameter, D*, between 0 and 0.5 was found to obey a $Ri^{-3/2}$ power law. The entrainment rate is independent of D* between 0 and 0.5 for a range of Richardson numbers from 3 to 25. This is consistent with the behavior of the buoyancy-reversing thermal in an unstratified environment observed by Johari (1992).

Acknowledgments

I am glad that Dr. A. Cotel was my advisor. She was not only my advisor but also my best friend. Her friendship over the past two years have made my time quite enjoyable. Under her supervision, I have developed a physical understanding of fluid mechanics and enriched my knowledge of turbulent flows. Special thanks must go to her.

I thank Dr. R.W. Derksen for his valuable comments on my thesis. I am very appreciative of his help.

I would like to thank the following people for their contributions:

- Irwin Penner and John Finken, for helping me to build the experimental apparatus;
- Kim Majury, for providing the video equipment;
- Gayle Ferguson, for juggling with budgets and making sure I got my paychecks;
- Kusum Vyas, Evelyn, and Bev Dunlop, for assistance in the office.

This work was supported by the Natural Sciences and Engineering Research Council of Canada (research grand and Dr. Cotel start-up funds from the University of Manitoba).

I would also like to thank my mother, Changling Sun's support.

TABLE OF CONTENTS

LIST OF TABLES

LIST OF FIGURES

Chapter 1. Introduction

Most fluid motions in the atmosphere and oceans are turbulent, and strongly influenced by the dynamics of stratified flows. It is therefore essential to understand their dynamics in order to comprehend the environment. The objective of this thesis is to extend our understanding of the fundamental physical processes involved in stratified turbulent flows. In stratified flows, turbulent entrainment, being the first step in mixing, plays a central role. Entrainment controls the growth and decay of convective clouds in many ways. Laboratory experiments and numerical models are necessary to understand the complex flow field of atmospheric convection.

This dissertation focuses on understanding the turbulent entrainment of a thermal impinging on a stratified interface. A direct application of this work is to study the interaction between clouds and the tropopause. The tropopause is a very thin layer between the troposphere and stratosphere, and also represents the location of a discontinuity in the temperature profile. It is located about 11km above the earth's surface. The troposphere is the layer of the atmosphere below the tropopause, accounting for more than 80% of the mass and virtually all of the water vapor, clouds, and precipitation in the earth's atmosphere. The stratosphere is the layer of the atmosphere above the troposphere between 10 and 40km. They together account for about 99.9% of the atmospheric mass (Wallace & Hobbs, 1977). Accurate modeling of mass transport across the tropopause is necessary to understand the concentration of ozone and other chemicals in the stratosphere. Some cumulus clouds contain pollutant air and penetrating through atmospheric inversions may affect the ozone budget. The quantity of pollutants penetrating into the stratosphere might reduce the equilibrium concentration of ozone, thereby allowing more ultraviolet radiation to reach the earth's surface (Wallace & Hobbs, 1977). This is considered to be an important factor in the issue of global warming. It is necessary to gain further insight into stratified entrainment to yield better models of atmospheric dynamics in global climate models as well as weather forecasts. Turbulence is not accurately represented in present-day models, especially for geophysical applications.

Among turbulent flows, the motion of buoyant fluid known as 'thermal' has been studied theoretically, experimentally and computationally for several decades. However,

only preliminary work has been done to study the interaction between a stratified interface and a thermal, and no entrainment measurements have been performed for this specific case.

The term "thermal" is used to denote a parcel of isolated buoyant fluid suddenly released from rest, which subsequently moves under the action of buoyancy forces alone. Thermals, easily observed as cumulus clouds in the atmosphere, have been measured in shape and motion. They are buoyancy-driven convection eddies which generate most of the turbulence in the unstable atmospheric boundary layer (Young, 1988). An isolated thermal is the ultimate form of convective elements in the atmosphere (Woodward, 1959). From the motion of cumulus clouds, it appears that convection, which is produced by buoyancy forces, consists largely of more or less isolated masses of buoyant air rising into and mixing with their surroundings (Scorer, 1957). The general motion of a thermal is similar to a vortex ring (Turner, 1986). Moreover, the surface of a thermal has a 'cauliflower' pattern characteristic of cumulus clouds. A thermal is characterized by its total buoyancy force and does not possess any circulation, kinetic energy, or momentum at the moment of release. The circulation is generated entirely by buoyancy after the thermal is released. The horizontal scales of thermal circulation range around 1.5 times the depth of the convective boundary layer (Caughey & Palmer, 1979). The classical view (Scorer, 1957) indicated that the entrainment and mixing of a thermal take place over the advancing front of the thermal, then the mixed fluid parcels are taken to the center of the thermal by the vortex core rotation. However, using laser-induced fluorescence, Johari (1992) found that environmental fluid is first mixed at the center of

the thermal. His description is based on the notion of entrainment and mixing by large eddies (Roshko, 1976). Entrainment in thermals is accomplished through engulfment of fluid in the rear of thermals because the induced velocity from the vorticity field causes ambient fluid to enter the backside of the thermal. Even though small eddies around the front and sides of the thermal also participate in the entrainment process, the bulk of entrained fluid comes from large-scale motions of the vortex core. The volume of fluid entrained by small scale eddies is negligible compared to the contribution from large-scale motions (Johari, 1992). It is believed that the motion within a thermal is composed of a rising motion in the middle and a descending one on the sides, similar to a vortex ring (Woodward, 1959 and Turner, 1963). A thermal has a spreading angle of about 33 degrees while the diameter increases linearly with vertical or downstream distance from the source (Figure 1). The advancing front of a thermal has traditionally been used for measurements since it is a relatively distinctive point (Johari, 1989). A self-similar thermal has a width of about half the distance the front traveled (Johari, 1992).

Taylor first described the entrainment hypothesis at the Pacific Science Association meeting in 1949; however, Batchelor (1954) gave a wider exposure through a review lecture. The basic form of this hypothesis is that the mean inflow velocity across the edge of a turbulent flow is assumed to be proportional to the local characteristic velocity (Figure 2). For a jet, the entrainment velocity is proportional to the centerline velocity. The velocity of a thermal rising in an unstratified environment is its characteristic velocity. The total volume inflow depends on the surface area, the geometry and the dynamics of the flow (Turner, 1986).

Scorer (1957), Woodward (1959), and Turner (1963) performed tank experiments involving heavy brine parcels sinking through fresh water. They observed that the diameter increases linearly with vertical distance from the source. Their results seemed to confirm the applicability of similarity solutions. The basic results of dimensional analysis have been supported by laboratory experiments from which numerical values of the various constants have been obtained, and also by more detailed numerical calculations. For an isolated thermal released in a water tank, there are simple dimensional laws which are as follows (Turner, 1964):

$$r = \alpha z \tag{1}$$

$$w = \frac{dz}{dt} = C(g'r)^{1/2} \tag{2}$$

$$g' = \frac{g(\rho_1 - \rho)}{\rho_1} \quad , \tag{3}$$

where r is the half-width of the thermal, z is the height of the front of the thermal, α is a dimensionless constant, w is the velocity of the thermal, C is another dimensionless constant, g' is the buoyancy acceleration due to the density difference ($\rho_1 - \rho$), ρ and ρ_1 are the densities inside and outside of the thermal, respectively, and g is the acceleration due to gravity. In the case of a thermal moving through a uniform ambient fluid, it is shown experimentally that C and α remain constant during a single experiment, with values of 1.2 and 0.25, respectively. From the thermal geometry and assuming potential flow in the surroundings, the values of C and α can be determined without requiring any

information about the flow inside the thermal (Turner, 1964). On the other hand, the buoyancy force, F*, remains constant for any rising thermal. There is a clear dependence of the various parameters on the height z and the buoyancy force F* (Turner, 1973). The velocity, size and acceleration due to buoyancy are as follows:

$$w \propto F^{*1/2} z^{-1} \tag{4}$$

$$r \propto z \tag{5}$$

$$g' \propto F^{*} z^{-3} \quad . \tag{6}$$

Grabowski and Clark (1991 and 1993) used two and three-dimensional numerical experiments to simulate thermals and study the environment-boundary instability. The subject of their studies, namely, the cloud-environment interface instability, is considered by them a primary entrainment mechanism. The buoyancy gradient between the thermal and its environment generates vorticity sheets at the leading-edge boundary surrounding the rising thermal. Simulations discussed in those papers show that a shear layer tangential to the thermal-environment interface develops as the thermal rises, with upward motion inside the thermal and downward motion in the environment. This shear layer is associated with baroclinic vorticity production by horizontal gradients of buoyancy (Grabowski and Clark, 1991). However, there are no known laboratory or field observations reporting similar structures.

In stratified turbulence, the interaction between stratified interfaces and turbulent flows is a critical problem. Some experiments have shown that the entrainment rate declines in general with increasing stratification. It is observed that the relationship

between the entrainment rate and the Richardson number obeys a power law (Turner, 1973) when the Richardson number is between one and a few hundreds. The relationship is often defined as:

$$\frac{w_e}{w_l} = cRi^{\alpha} \quad , \tag{7}$$

where w_e is the entrainment velocity across the interface, w_l the characteristic velocity of the impinging turbulent flow, c and α are dimensionless constants. The Richardson number (the ratio of potential energy to kinetic energy) is defined in terms of the impinging turbulence quantities:

$$Ri = \frac{g'\delta}{w_l^2} \tag{8}$$

$$g' = \frac{\Delta\rho g}{\rho} \quad , \tag{9}$$

where g' is the buoyancy acceleration due to the density difference $\Delta\rho$, g is the acceleration of gravity, $\Delta\rho$ is the density difference across the interface, ρ is the density of one layer fluid, δ is the length scale of the incident turbulence at the interface, w_l is the characteristic velocity of the turbulence (Figure 3). For Ri<1, the kinetic energy of the largest eddies is greater than the potential energy investment in engulfing a tongue of fluid, so there is little or no effect of stratification on entrainment. When the Richardson number is very large, the interface becomes flat. The diffusion becomes the dominant

entrainment process and the potential energy can no longer affect the entrainment. Therefore, the entrainment rate becomes independent of Ri (Breidenthal and Baker, 1985).

The entrainment velocity, w_e, represents the rate at which the interface is rising due to entrainment of upper layer fluid into the turbulent flow, emerging from the lower layer (see figure 3). The dimensionless entrainment rate is defined as the ratio of the entrainment velocity w_e to the characteristic velocity w_t. In the literature, the value of the entrainment exponent α has been found to be -1/2, -1, -3/2 or in one case -2. For a vortex ring (Linden, 1973) and a plume (Kumagai, 1984), α was found to be close to -3/2. For a jet impinging on a stratified interface (Cotel et al., 1997), α was measured to be –1/2. Turner (1973) also found that the value of α seemed to depend on the Schmidt or the Prandtl number if the stratification agent was heat rather than salt for stirring grid turbulence. The Schmidt number (Sc) is

$$Sc = \frac{\nu}{D_m} , \tag{10}$$

where D_m is the molecular diffusivity and ν is the kinematic viscosity. The Prandtl number (Pr) is

$$Pr = \frac{\nu}{D_T} , \tag{11}$$

where D_T is the thermal diffusivity. When the Richardson number is less than seven, the value of α equals -3/2. If Ri>7, the value of α remains -3/2 for salt stratification, but becomes -1 for heat stratification (Turner, 1973). Cotel and Breidenthal (1997) suggested

that the persistence of the entraining eddies is a critical parameter in determining the entrainment regime, in addition to the conventional parameters such as Richardson, Reynolds and Schmidt numbers. The dimensionless vortex persistence parameter T is defined to be the number of rotations a vortex makes during the time it moves its own diameter with respect to the interface (Cotel and Breidenthal, 1997). T is proportional to the ratio of the rotational to the translational speed of the entraining eddy. The translational speed is the speed at which the eddy is moving with respect to the interface. The rotational speed is unambiguous to any inertial observer. T is independent of Ri, Re or Sc, since they all can be varied separately while T is held constant. Based on the value of the persistence parameter for thermals estimated to be close to unity, the entrainment rate is predicted to be proportional to $Ri^{-3/2}$ for a thermal impinging on a thin interface, for a range of Ri greater than 1, but less than that at which the interface becomes flat, i.e. at $Ri = Re^{1/4}$ (Cotel and Breidenthal, 1997).

Little laboratory work has been done on thermals interacting with a stratified interface. In early 1960s, Richards (1962) and Saunders (1962) observed the penetration of thermals through an interface between different density fluids. Richards (1962) found the actual velocity w_l of the front of a thermal measured at the interface to follow the laws:

$$w_l = \frac{k_l}{2h} \tag{12}$$

$$z = n_l r \tag{13}$$

$$z^2 = k_1 t \tag{14}$$

$$k_1 = C_1 n_1^{3/2} \left(\frac{gM}{\rho_1} \right)^{1/2} , \tag{15}$$

where z is the distance traveled, r is the half-width of the thermal, t the elapsed time, h the height of the interface, M the mass excess which is the difference between the masses contained within and displaced by the thermal while in the surrounding fluid, and ρ_1 the density of the displaced fluid. The parameter n_1 is constant for thermals; however, it varies between different runs over the range 1.9 to 7.5. C_1 has roughly the same value for all thermals, 0.73.

In our laboratory experiments, two kinds of thermals were investigated. "Classical" thermals are produced by positive buoyant forces. This is the first step in mimicking the atmospheric convective case. However, evaporative cooling and latent heat release all affect the dynamics of clouds in the atmosphere. Evaporative cooling occurs when dry environmental air is entrained into positively buoyant cumulus clouds and changes the positively buoyant clouds to negatively buoyant clouds. Latent heat is released during the phase changes at constant temperature in a cloud environment and generates extra buoyancy (Wallace & Hobbs, 1977). Our next step focuses on the effects of evaporative cooling. In order to simulate cloud conditions more closely, buoyancy reversal has been used in the laboratory to simulate evaporative cooling. When atmospheric convection develops in the troposphere, airflows of various scales, from small scale turbulence to large eddies, initiate entrainment and detrainment and create mixing between convective

air and the environment (Betts, 1973; Blyth et al, 1988; Bretherton & Smolarkiewicz, 1989; Taylor & Baker, 1991). The mixing process reduces the buoyancy of the cloud air very efficiently by evaporating liquid water droplets within clouds. In other words, the cloud air quickly becomes negatively buoyant in the troposphere because of mixing with environmental dry air (Hu, 1998). Buoyancy reversal has been considered to have a dramatic effect on the global motions of clouds, but it has less effect on the entrainment rate and mixing of buoyant fluid (Johari, 1992; Grabowski and Clark, 1993). A few experimental and numerical studies have investigated effects of evaporative cooling. Buoyancy reversal, which is a result of evaporative cooling, influences the entrainment process if the magnitude of the reversal is comparable to the initial stratification (Shy and Breidenthal, 1990) via a "cloud-top entrainment instability" proposed by Deardoff (1980) and Randall (1980). The concept of "cloud-top entrainment instability" assumes a positive feedback between the buoyancy reversal due to evaporative cooling and the entrainment rate. Grabowski (1995) argues that the buoyancy reversal affects the entrainment in two different ways. First, buoyancy reversal directly enhances the kinetic energy of small-scale entraining eddies, so the enhanced entrainment is thought to occur when the magnitude of the reversal is comparable to the initial stratification. Second, buoyancy reversal indirectly leads to more entrainment and mixing through large-scale eddies entraining air into cloud. In other words, enhancement of entrainment occurs through the enhancement of global flow structures. Furthermore, Turner and Yang's (1963) early laboratory experiments found that the rate of entrainment at the top of stratocumulus clouds was not enhanced significantly by modest buoyancy reversal. There is a clear distinction between the dramatic effects of buoyancy reversal on the

overall dynamics on one hand and small effects on the dynamics of entraining eddies on the other hand as observed by Johari (1992) in the laboratory and numerically by Grabowski (1995).

According to Johari (1992) and Grabowski and Clark (1993), the entrainment should not be influenced dramatically by buoyancy reversal as long as it is weak. Moreover, the entrainment rate should decrease in general with increasing stratification as for positive buoyant thermals. However, no one has tested the effect of evaporative cooling in the case of impinging turbulence on a stratified interface.

Most of previous studies have looked at thermals in a homogeneous environment (Scorer, 1958; Woodward, 1959; Turner, 1964 and Johari, 1992). However, in the atmosphere, stratification is ubiquitous. Turbulence interacting with stratified interfaces plays a critical role in global atmospheric dynamics. Therefore, a simple, thin stratified interface was chosen to be investigated in the laboratory.

A water tank with a thermal release mechanism was used for the experiments. The laboratory experiments and results for the classical thermals impinging on a stratified interface are presented in chapter 2, and results for the buoyancy reversal case are in chapter 3. Finally, the summary and conclusions are presented in chapter 4.

Chapter 2. Thermals Impinging on a Stratified Interface without Buoyancy Reversal

2.1 Experimental Apparatus

The main problem in the creation of thermals in the laboratory is the development of a satisfactory release device with which reliable and repeatable thermals can be obtained. An ideal mechanism for releasing thermals would simulate the atmospheric release process as closely as possible. However, the atmospheric release process is not very well understood and therefore difficult to reproduce in a laboratory setting. Furthermore, thermals are very sensitive to initial disturbances and can have distinctly different trajectories due to small variations in the release process. This has to be taken into

consideration in the designing phase. One of the techniques is to invert a thin hemispherical cup filled with the thermal fluid, either from the top or the bottom of the tank (Scorer, 1958). Another method is to use a cylinder reservoir filled with buoyant fluid, and the lid of the chamber to be withdrawn suddenly to release the thermal from rest (Turner, 1963). In our experiments, the latter technique was adopted.

The material of the tank walls consists of chemically resistant lucite to give an unobstructed view of the flow. Thermals are released from the bottom of the tank as the rising clouds in the atmosphere. The apparatus is sketched in figure A in the Appendix. The parts of the apparatus are shown in table A and figures A-1 to A-10 (see Appendix). The dimensions of the tank are 12" x 12" x 27" in height. In order to create enough entrainment to be measured accurately and to minimize wall effects, a vertical cylinder of 2.5" inside diameter, 1" height and 1/8" wall thickness was designed and built (Figure A-9). It is located at the bottom of the tank and covered by a thin, horizontal sliding stainless steel lid of 10½" length, 3½" width, and 1/16" thickness (Figure A-8). A flat rectangle was cut out on the lower part of the right-side wall (Figure A-3) to pull the lid outward. The induced flow effects from the sidewalls were small because the width of thermals at the interface was less than forty percent of the tank's width (Johari, 1992). For the purpose of generating a thin stratified interface, the tank is separated into two chambers by a thin, horizontal sliding stainless steel plate 12" width, 16" length, and 1/16" thickness (Figure A-7) which is located half way up the tank. The left-side wall, front and back walls are slotted in for sliding the steel plate (Figure A-1 and A-2). The steel plate is pulled outward through the right-side wall (Figure A-3). The two holes in

the bottom of the tank are designed to drain the fluid (Figure A-4). O-rings seals are used to prevent leaking (Figure A-5 and A-6). This experimental apparatus was tested before the experiments were undertaken. The leaking problem from one side of the tank was prevented by using vacuum grease.

2.2 Experimental Techniques

2.2.1 Set Up

The complete experimental set-up is shown in figure 4. Two fluids of different salt concentrations are used to represent the top and bottom layers. The density of the lower layer fluid ρ_B is greater than that of the upper layer fluid ρ_A. The release mechanism is as follows. A cylinder, 2.5" in diameter and 1" high, is located at the bottom of the tank. Once the cylinder is filled with a mixture of pure water and water-soluble dye, the lid is slid back over the cylinder. Then, the lower section of the tank is filled with a fluid of density ρ_B. The sliding plate is pushed in, and finally a fluid with density ρ_A is poured into the upper section. The sliding plate and the lid are used to minimize mixing between the different fluids before a run. The density of the thermal ρ_t is always less than both ρ_B and ρ_A.

2.2.2 Experimental Procedure

First, the sliding plate, located in the middle of the tank, is pulled out. In order to obtain sufficient entrainment and to minimize wall effects, the tank is then slowly drained so that the interface is positioned at the desired level. The initial level of the interface is set at 12"; the final position is between 8" and 12" from the tank bottom, depending on

different runs. The interface remains thin throughout the draining process. Then, the lid above the cylinder is withdrawn to begin a run. Considerable attention is necessary at this stage so that no initial circulation is imposed on the thermal. Experiments were recorded by using a combination of a TM-920 Video Monitor, a TK-1280U video camera fitted with a TV-200M COSMICAR Lens, and a SONY VCR.

2.3 Experimental Results

The evolution of a thermal rising towards the interface is shown in a sequence of photographs from a single run (Figure 5a-f). The initial interface is marked with dots in the photographs. The interface is thin compared with the thermal eddy size. The buoyant thermal fluid is released from the cylinder at the bottom of the tank (Figure 5a). Before the thermal impinges on the interface, the largest eddies are responsible for controlling the rate of momentum and mass transport, because they have a greatest velocity, and, equally importantly, the greatest range (Roshko, 1976). A wake can be observed behind the thermal due to release procedure (Figure 5b). At this stage, the thermal becomes self-similar as the width of the thermal is about half of the distance the front traveled (Johari, 1992). The thermal penetrates through the interface, rebounds from it and spreads laterally (Figure 5c). At this point in the experiment, the entraining eddy may not be the largest one because of stratification. The interface rises by a certain amount due to turbulent entrainment across it (Figure 5d). The thermal collapses (Figure 5e). Finally, the thermal entrainment process is finished and the interface becomes flat (Figure 5f). The average entrainment velocity is

$$w_e = \frac{H_{ir}}{t_{ir}} , \qquad (16)$$

where H_{ir} is the change in interface height due to thermal entrainment measured at $t=t_{ir}$. t_{ir} represents the duration of the entrainment process, from the time the thermal is released until the thermal stops entraining fluid from the upper layer. A stopwatch is used to record the different times. The thermal velocity is

$$w_l = \frac{d_{tr}}{t_{tr}} , \qquad (17)$$

where d_{tr} is a distance of 2cm just below the interface. t_{tr} is the time the thermal traveled the distance d_{tr} recorded with a stopwatch so that w_l represents the thermal velocity just below the interface. The height of the interface and the distance traveled by the thermal are measured visually from a ruler on the side of the tank. The width of the thermal δ is measured just before the thermal impinges on the interface (Figure 3). For all experiments, the interface is reached by a thermal in a few seconds, but the entrainment process at the interface takes at least 40 seconds.

Groups of data (Table 1) have been obtained from different runs. The dimensionless entrainment rate w_e/w_l versus the Richardson number Ri is shown in log-log plots (Figure 6a-c). The entrainment rate w_e/w_l is the velocity at which the interface is rising normalized by the measured thermal velocity as it approaches the interface. The Richardson number is based on the density difference as defined earlier in the introduction. In case 1 (Figure 6a), $\Delta\rho$ is equal to $\rho_B-\rho_A$, the density difference between the upper and the lower layer and ρ is ρ_B, the density of the lower layer fluid. In case 2

(Figure 6b), $\Delta\rho$ is the same as in case 1, but ρ is ρ_A, the density of the upper layer fluid. In case 3 (Figure 6c), $\Delta\rho$ is equal to ρ_A-ρ_t, the density difference between the thermal and the upper layer fluid, and ρ is ρ_A, the density of the upper layer fluid. We assumed the density of the thermal doesn't change during a single run in case 3. From Figure 6a-c, we found that the entrainment rate declines with increasing Richardson number as equation 7. The value of the exponent, i.e. the slope is determined by curve fitting to be between –1.5 and –1.52. There is about $\pm$10%–15% error due to lack of accuracy when measuring the time.

We define the Reynolds number

$$Re = \frac{w_l \delta}{\nu} \quad . \tag{18}$$

Re is based on the thermal quantities: its diameter δ, velocity w_l and the kinematic viscosity ν. The value of the Reynolds number for all runs is around 10^4.

2.4 Discussion

The results are similar to those obtained for stirring grid turbulence (Turner 1973) and a plume impinging on a stratified interface (Kumagai 1984). There is almost no entrainment at high Richardson number. It is not recorded on Figure 6a-c, due to the lack of measurement accuracy for such small values of the entrainment rate. On the other

hand, no matter which density is used in the definition of the Richardson number, the same results are obtained.

The results confirms the prediction that the entrainment rate of a thermal impinging on a stratified interface is proportional to $Ri^{-3/2}$ (Cotel and Breidenthal, 1997). The present experiments reinforce the importance of the persistence parameter. As we mentioned in the introduction, a thermal is non-persistent. Let us compare a thermal with a vortex ring. Assuming the Ri, Re and Sc numbers are the same for both cases, the creating process, i.e. momentum or buoyancy, does not determine the entrainment regime. In the cases of the vortex ring and the thermal, the value of the persistence parameter is the same, and the same entrainment law is measured. For a jet and a plume, the persistence parameter and the entrainment regime are different, the jet is persistent, whereas the plume is subject to high fluctuations (Dai et al., 1994), and is therefore non-persistent. There is a direct correlation between the value of the persistence parameter and the entrainment regime, when the other parameters are the same. The creation mechanism of either buoyancy or momentum is not significant in determining the entrainment rate.

A fully accurate laboratory simulation of atmospheric thermals would include the effect of evaporative cooling and latent heat. We choose to add the effect of buoyancy reversal to a thermal in order to simulate evaporative cooling in the laboratory. Evaporative cooling is more practical to simulate in the laboratory than latent heat release at this stage of our study.

Chapter 3. Evaporative Cooling Effects on Thermal Entrainment

Evaporative cooling happens when a positively buoyant cloud parcel becomes negatively buoyant due to a change in density because the evaporation of liquid water droplets within a cloud causes cooling (Johari, 1992). For instance, atmospheric moist convection is an example of a buoyant reversing system, because mixing of positively buoyant cloudy air and dry environmental air usually leads to the formation of negative buoyancy (Grabowski, 1995).

3.1 Buoyancy Reversal Parameter

In order to simulate the density changes accompanying evaporative cooling in a water tank, Johari (1992) used mixtures of ethyl alcohol and ethylene glycol as thermals were released from the bottom of the tank. The same chemicals were used in the experiments of Turner (1966). Johari (1992) found that the behavior of thermals depends strongly on a dimensionless parameter, called the buoyancy reversal parameter:

$$D^* = \frac{\rho^* - \rho(0)}{\rho(0) - \rho(1)} \quad . \tag{19}$$

The density is a function of the volume fraction of released thermal fluid. Thus $\rho(0)$ is the density of the environment and $\rho(1)$ is that of the initial thermal fluid. The peak density of a given alcohol-glycol mixture is ρ^*.

The same technique was used in our experiments. Several curves (Figure 7) describe the density of thermals against the volume fraction of thermal fluid P. The horizontal line represents the density of the lower layer fluid initially surrounding the thermal. The curves above and below this line show the thermal with negative and positive buoyancy, respectively. The pure thermal fluid is represented by P=1, and the ambient fluid by P=0. When P equals P*, the alcohol-glycol mixture reaches its peak density ρ^*. A thermal would have then maximum negative buoyancy. The dimensionless parameter D* (equation 19) determines the intensity of buoyancy reversal. In the absence of any buoyancy reversal, D*=0. Thermals rise continuously when D* is less than 0.5. Within this regime, thermals do not stop or turn back even though they decelerate. They also leave some fluid behind in their wake. For the values of D* close to 0.5, thermals detrain

a large volume of fluid. In the regime of D* between 0.6 and 0.9, thermals travel a certain distance and break into two parts, one travelling upwards and the other downwards. Thermals always descend back toward the bottom of the tank after rising a short distance for D* greater than 1. The thermals in this regime do not develop very far and only penetrate a very short distance (Johari, 1992). In general, the trajectory of thermals with buoyancy reversal depends strongly on D* as mentioned above, and the "evaporating" thermals do not penetrate as far as thermals without buoyancy reversal.

The range of D* for the present experiments is from 0 to 0.5. Within this range, thermals rise to the top of the tank and do not break into two parts or turn down shortly after having been released, as discussed above. There is little amount of entrainment across the interface when the range of D* is greater than 0.5, so that no accurate measurements could be performed. We chose to restrict the range of D* so that the thermals produced are representative of the real atmospheric case (Siems et al., 1990).

Johari's (1992) experiments show that the molecular-scale mixing features of these thermals are similar to that of rising thermals without buoyancy reversal as long as these thermals maintain upward motion, even though the trajectory is strongly affected by D*. It implies that buoyancy reversal does not influence the fundamental mixing and entrainment dynamics of convective elements, as long as the thermal is rising. The same result was also found in numerical experiments. Grabowski & Clark (1993) and Grabowski (1995) did numerical experiments on thermals with and without buoyancy reversal. They believe that entrainment in the numerical experiments is driven by the

baroclinic instability, and not by the buoyancy reversal process. Then, they suggested that buoyancy reversal associated with evaporative cooling affects the overall flow evolution, but has small effects on the dynamics of the entraining eddies. In other words, buoyancy reversal has little effect at the initial stages of cloud development, but the entrainment rate is likely to change significantly when the buoyancy reversal becomes very strong.

3.2 Experimental Procedure

The apparatus is similar to that used for the experiments of the classical thermals (Figure 4). Two fluids with different densities represent two layers separated by a stainless steel sliding plate in the middle of the tank. The upper layer fluid is a mixture of water and alcohol with density ρ_A. The content of alcohol varies from 0.04% to 0.17% in this layer for different runs. The lower layer fluid is pure water with density ρ_B, greater than ρ_A. The release mechanism is a cylinder covered with a small sliding lid to prevent the alcohol-glycol mixture from mixing with the surrounding fluid. The mixture is visualized by adding water-soluble dye. The densities of the two fluids, ρ_A and ρ_B, are always greater than the thermal density ρ_t.

The first step is to fill the small cylinder at the bottom of the tank with an alcohol and glycol mixture and cover it with the lid. In order to construct a simple discontinuous stratification in the environmental fluid, the lower section of the tank is filled with water

and covered with the horizontal plate, then a water and alcohol mixture is poured into the upper section. Withdrawing the plate carefully yields an interface that is thin compared with the thermal size. To ensure that thermals are reaching the interface without wall effects, the interface is lowered by draining the water from the lower chamber, before a run. The appropriate position was found to be at a height between 5.5" to 7.5" from the bottom of the tank for different runs. The draining process must be slow to avoid disturbing the interface. Then, the lid is pulled out to begin a run.

3.3 Results

The buoyant thermal fluid mixture rising from the cylinder at the bottom of the tank is shown in figure 8a. When the initial positively buoyant thermal begins to mix with the ambient fluid, the density of the thermal is increased but is still less than that of the lower layer. A partially negatively buoyant thermal is generated as shown in figure 8b. It appears that the negative buoyancy decelerates the thermal. The thermal continues to travel upwards because the total density of the thermal is still less than that of the environment and penetrates through the interface, rebounds from it and spreads laterally along the interface (Figure 8c). The behavior is not much different from classical thermals without buoyancy reversal for the range of D* between 0 to 0.5. The interface rises a certain amount because of turbulent entrainment of the upper layer fluid into the thermal (Figure 8d). The thermal collapsed after several seconds (Figure 8e). Finally, the thermal entrainment process is finished (Figure 8f). Similar measurement techniques

to the classical thermal case are used, the same quantities are measured, i.e., the instant width of the thermal, the velocity of the thermal and the entrainment velocity.

The volume ratio of alcohol to glycol in the initial thermals is 94% to 71% for different runs as shown in table 2. For instance, the ratio is 94% for the first run. One group of data of D*=0.214 is shown in table 3. The dimensionless entrainment rate w_e/w_l versus the Richardson number Ri is shown in six log-log plots (Figure 9a-e) and the value of the exponent is determined from curve fitting to be between –1.46 to –1.63. The entrainment rate w_e/w_l is defined as before. The entrainment rates clearly decline with increasing Richardson numbers (Figure 9a-e) for different values of D*. The relationship between the entrainment rate w_e/w_l and the dimensionless parameter D* between 0–0.5 is plotted in log-log plots for several values of the Richardson number (Figure 10a-c). The slope between w_e/w_l and D* is from 0.03 to 0.08 known by curve fitting. The error is of the order of $\pm$ 10%–20% due to lack of accuracy when measuring the time. The Reynolds number based on the thermal quantities at the interface is 10^4.

The possibility of buoyancy reversal between the lower and upper layer fluids has been tested. Data show no buoyancy reversal between those two layers.

3.4 Discussion

The results of the relationship between the entrainment rates and the Richardson numbers are similar to those for classical thermals. There is a difference in magnitude

for the entrainment rate with and without buoyancy reversal of a factor of 10 (Figure 11). This can be explained by the decrease in size and acceleration of the thermal due to buoyancy reversal. As seen in figure 8c, some of the thermal fluid is left behind as the thermal is rising. A net decrease in velocity is also easily observed. However, the difference does not influence the relationship between the Richardson number and the entrainment rate. The entrainment velocity at large Ri could not be measured due to low measurement accuracy. These results indicate that the relationship between the entrainment rate and the Richardson number follows the same power law for thermals with or without buoyancy reversal, impinging on a stratified interface.

The results in figure 10a-c demonstrate that the entrainment rates can be assumed to be independent of the buoyancy reversal parameter for $0<D^*<0.5$ for the case of thermals impinging on a stratified interface. This is in agreement with Grabowski and Clark (1993); the entrainment rate is constant in this range, so the effects of buoyancy reversal are negligible on the dynamics of entraining thermals when the buoyancy reversal parameter is small. These results are also supported by the result of Johari's (1992) laboratory experiments. The mixing and entrainment dynamics of convective elements do not depend on the presence of buoyancy reversal phenomenon as long as upward motion is maintained. Therefore, it is believed that buoyancy reversal does not significantly affect the rate of mixing between convecting fluid and its environment.

Moreover, Siems et al. (1990) analyzed soundings from atmospheric data on stratocumulus and trade cumulus clouds, taken from the FIRE (First ISCCP Regional

Experiment) experiment in 1987 and Joint Hawaiian Warm Rain Project experiment in 1985, respectively. They suggest that D* observed in stratocumulus is less than 1.3. The observations could not determine the value of the critical D* above which there is strong buoyancy reversal and unstable behavior as seen in the laboratory by Shy and Breidenthal (1990).

Chapter 4. Summary and Conclusions

Laboratory experiments provide a powerful tool for investigating the fundamentals of stratified turbulence, leading to new insight in natural atmospheric phenomena. The present experiments improve the current understanding of transport across the tropopause by making the first measurements of entrainment across an interface due to a rising thermal with and without evaporative cooling.

For thermals without buoyancy reversal, the entrainment rate was found to be proportional to $Ri^{-3/2}$ as predicted by Cotel and Breidenthal (1997). The effect of evaporative cooling on thermal entrainment was investigated in the laboratory. The entrainment rate was also found to be proportional to $Ri^{-3/2}$. In our experiments, the value

of the entrainment rate does not depend on the buoyancy reversal parameter D* for the range of 0–0.5. The buoyancy reversal parameter in the laboratory is of the same order as that in the atmosphere (Siems et al., 1990). The laboratory experiments represent a case of weak buoyancy reversal. There is a difference in magnitude (factor of 10) for the entrainment rate of the thermal with and without buoyancy reversal, due to the deceleration and the reduced size of the thermal in the buoyancy reversal case. The Richardson number ranged between 3 to 25, the Reynolds number was of the order of 10^4, and the Schmidt number was around 600 for the experiments performed.

The large differences in Reynolds and Schmidt numbers between the laboratory and the atmosphere are important issues for geophysical interpretation of laboratory results. The Reynolds number in the atmosphere around 10^8 to 10^9, is much larger than the Reynolds number in the laboratory of the order of 10^4. The results from laboratory experiments are expected to be applicable to the atmosphere, as long as the Reynolds number is above a critical value of order 10^3 called the mixing transition (Breidenthal & Baker, 1985) which is necessary for the development of small-scale turbulence. Furthermore, the entrainment rate of a jet impinging on a stratified interface was found to be independent of Reynolds number for Ri between 1 and 100 (Cotel, 1995).

The experiments reported here represent the first step in quantifying turbulent entrainment of thermals impinging on a stratified interface. The logical next step would be to include latent heat to completely simulate the atmospheric case in the laboratory. Also, the amount of mixing produced by a thermal penetrating in a stratified environment

needs to be quantified using laser-induced fluorescence. Particle image velocimetry measurements of the velocity and vorticity fields would be useful in determining the interface dynamics. These future steps would further our understanding of thermals in a stratified environment.

TABLE 1. Experimental data for thermals without buoyancy reversal case 1

Exp. Number	ρ_t (g/m^3)	ρ_u (g/m^3)	ρ_l (g/m^3)	δ (m)	W_l (m/s)	$\frac{w_e}{w_l}$	Ri
24	1004	1020	1036	0.09	0.050	0.00263	21.72
25	1004	1029	1036	0.085	0.052	0.00579	7.83
30	1005	1025	1036	0.09	0.057	0.00276	11.30
32	1006	1017	1036	0.09	0.053	0.00151	22.88
34	1005	1027	1036	0.09	0.064	0.00516	12.05
36	1006	1030	1036	0.09	0.044	0.01202	7.60
37	1006	1022	1036	0.085	0.062	0.00313	15.21
40	1006	1032.5	1040	0.085	0.074	0.00510	6.82
44	1004	1008	1028	0.08	0.071	0.00057	24.10
46	1005	1032	1036	0.09	0.052	0.01449	4.92

TABLE 2. Alcohol and glycol content in thermal mixtures

Number	Thermal density ρ_t (g/m^3)	D*	Alcohol (mm^3)	Glycol (mm^3)	%
1	963	0.053	160	170	94.1
2	968	0.078	150	170	88.2
3	976	0.16	200	250	80
4	980	0.214	125	169	74
5	984	0.471	110	152	72.4

TABLE 3. Experimental data for thermals with buoyancy reversal for $D^* = 0.214$

Exp. Number	ρ_t (g/m^3)	ρ_u (g/m^3)	δ (m)	w_l (m/s)	$\frac{w_e}{w_l}$	Ri
54	980	997	0.050	0.0235	0.00131	3.57
55	980	994	0.050	0.0229	0.00068	6.57
57	980	987	0.055	0.0195	0.00012	18.02
62	980	996	0.050	0.0235	0.00115	4.43

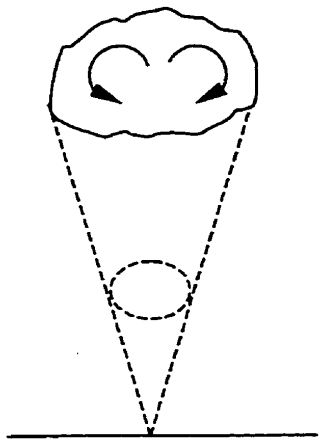

Figure 1. Sketch of a thermal

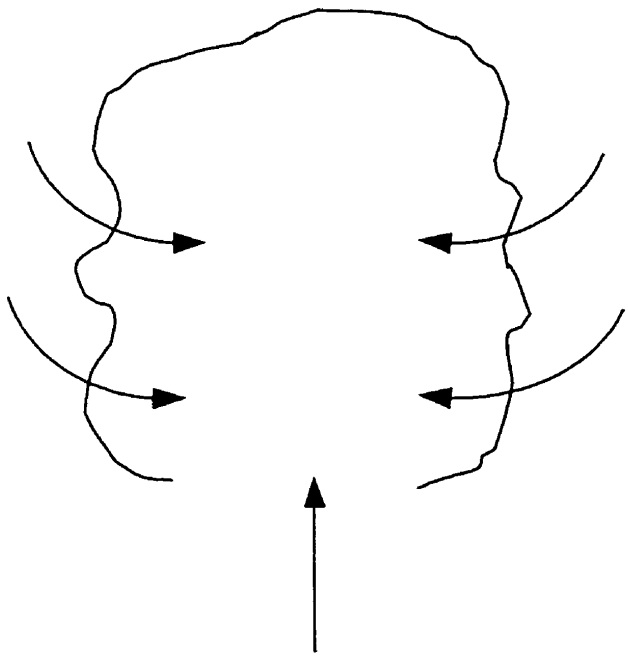

Figure 2. Cloud entrainment

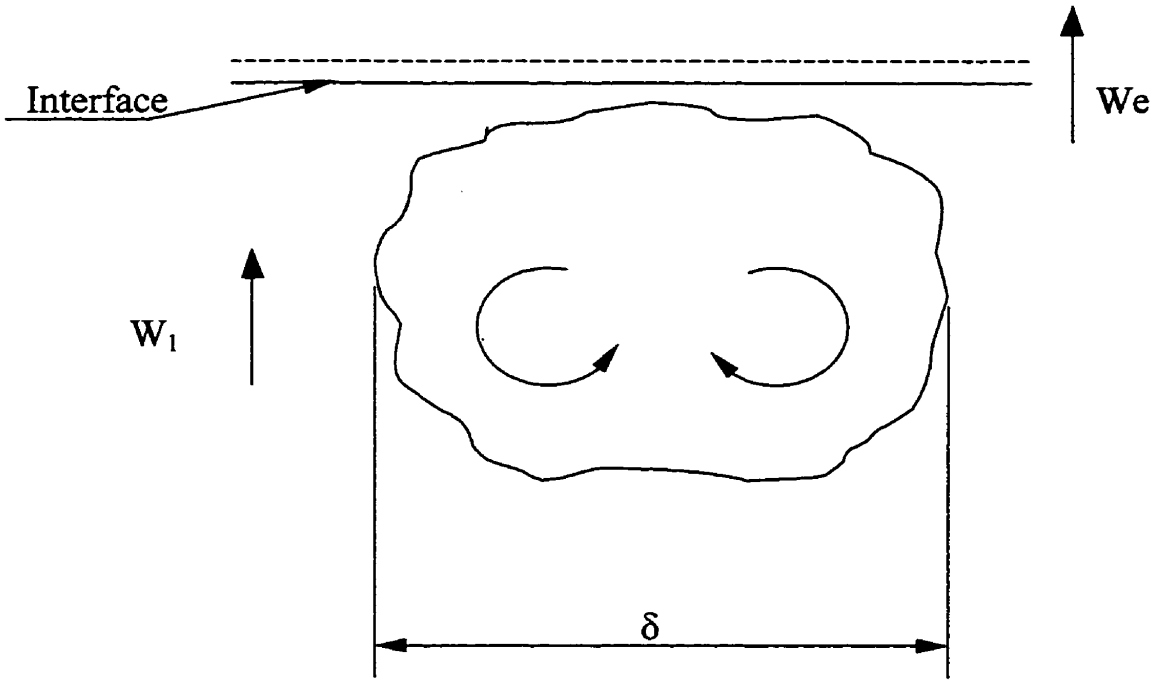

Figure 3. Schematic of a thermal impinging on a stratified interface

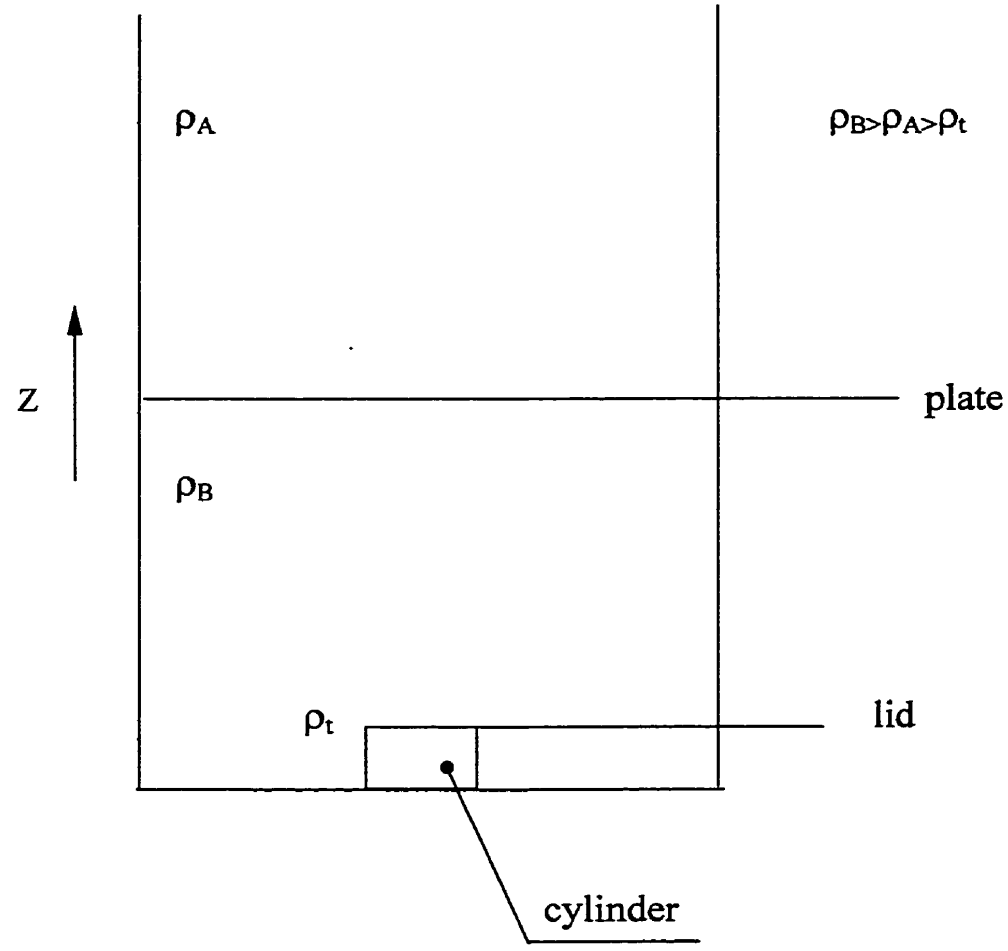

Figure 4. Sketch of the water tank

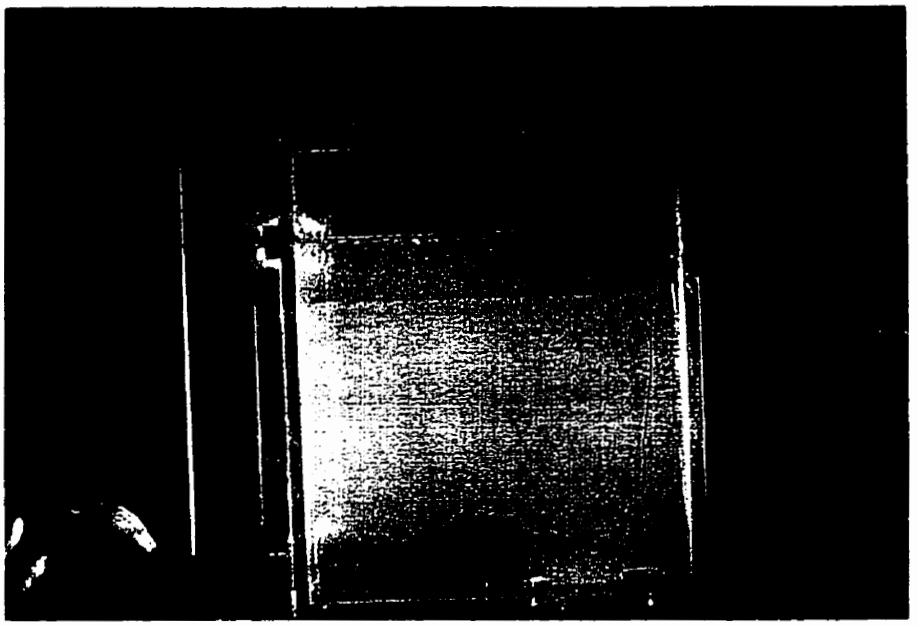

Figure 5a. Photograph of a classical thermal just after release

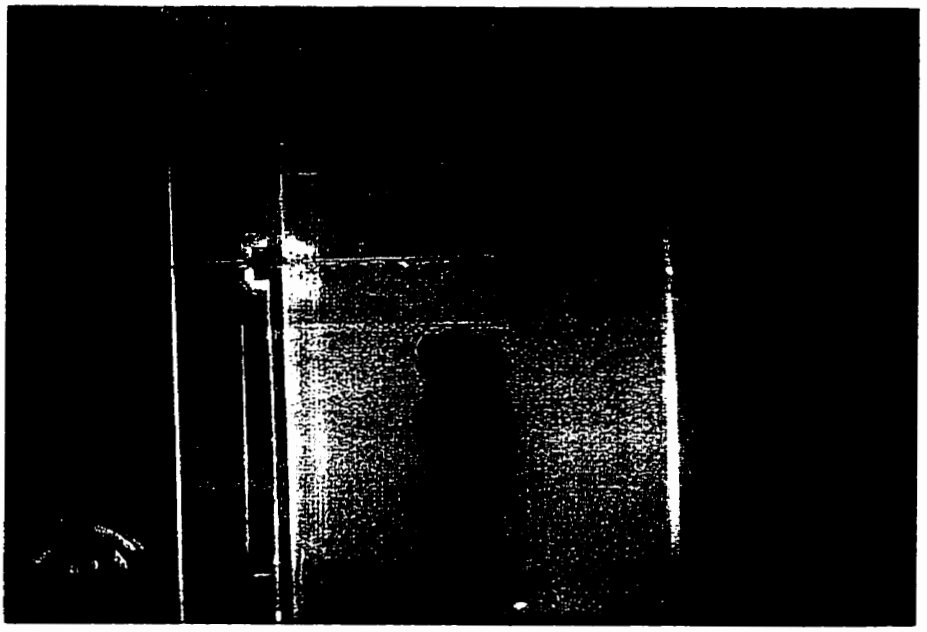

Figure 5b. Photograph of a classical thermal before impinging on the stratified interface

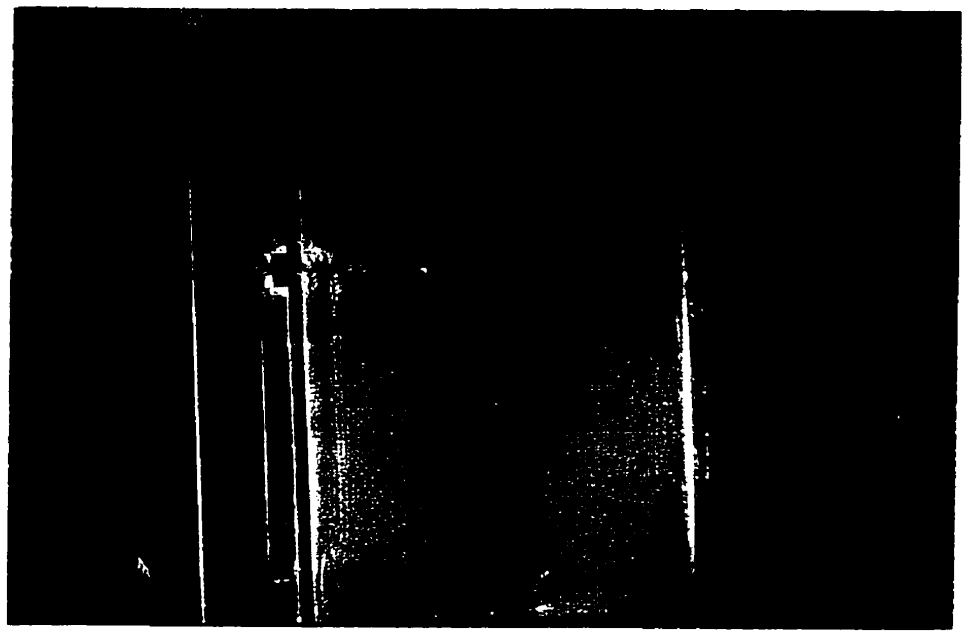

Figure 5c. Photograph of a classical thermal impinging on the stratified interface

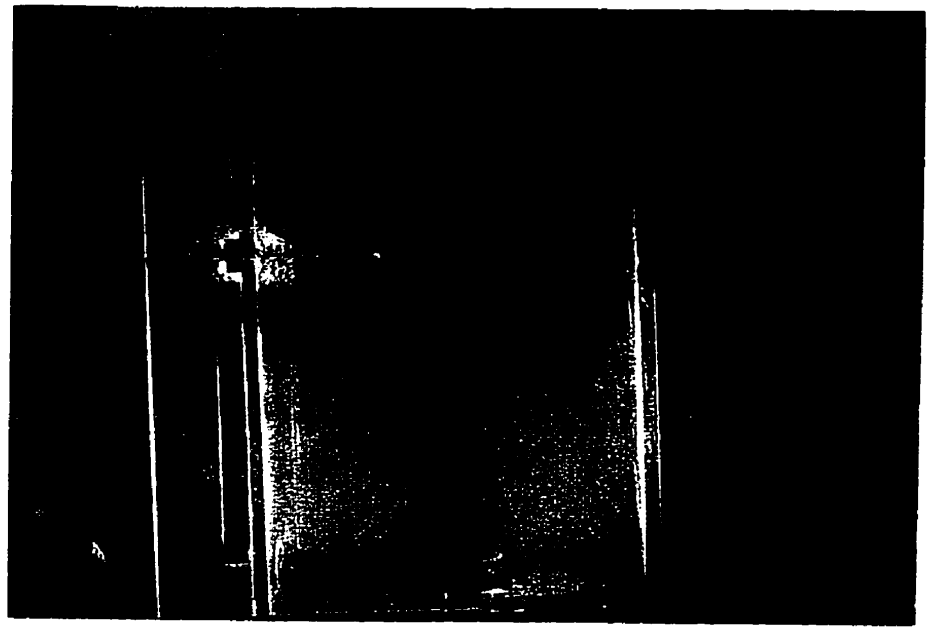

Figure 5d. Photograph of a classical thermal after impingement on the stratified interface

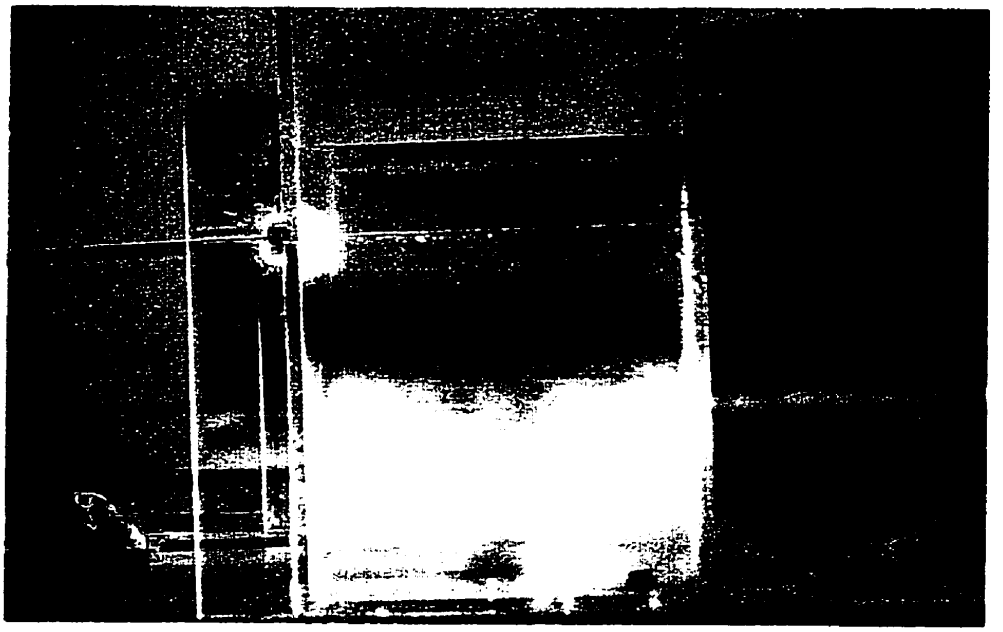

Figure 5e. Photograph of a classical thermal collapse after impingement on the stratified interface

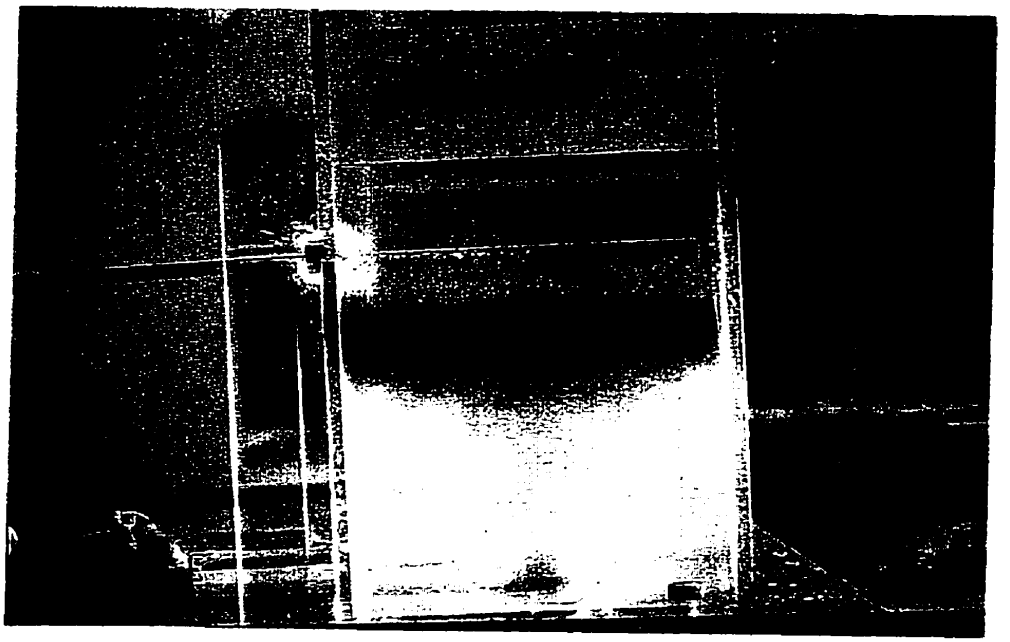

Figure 5f. Photograph of the final stage of a classical thermal

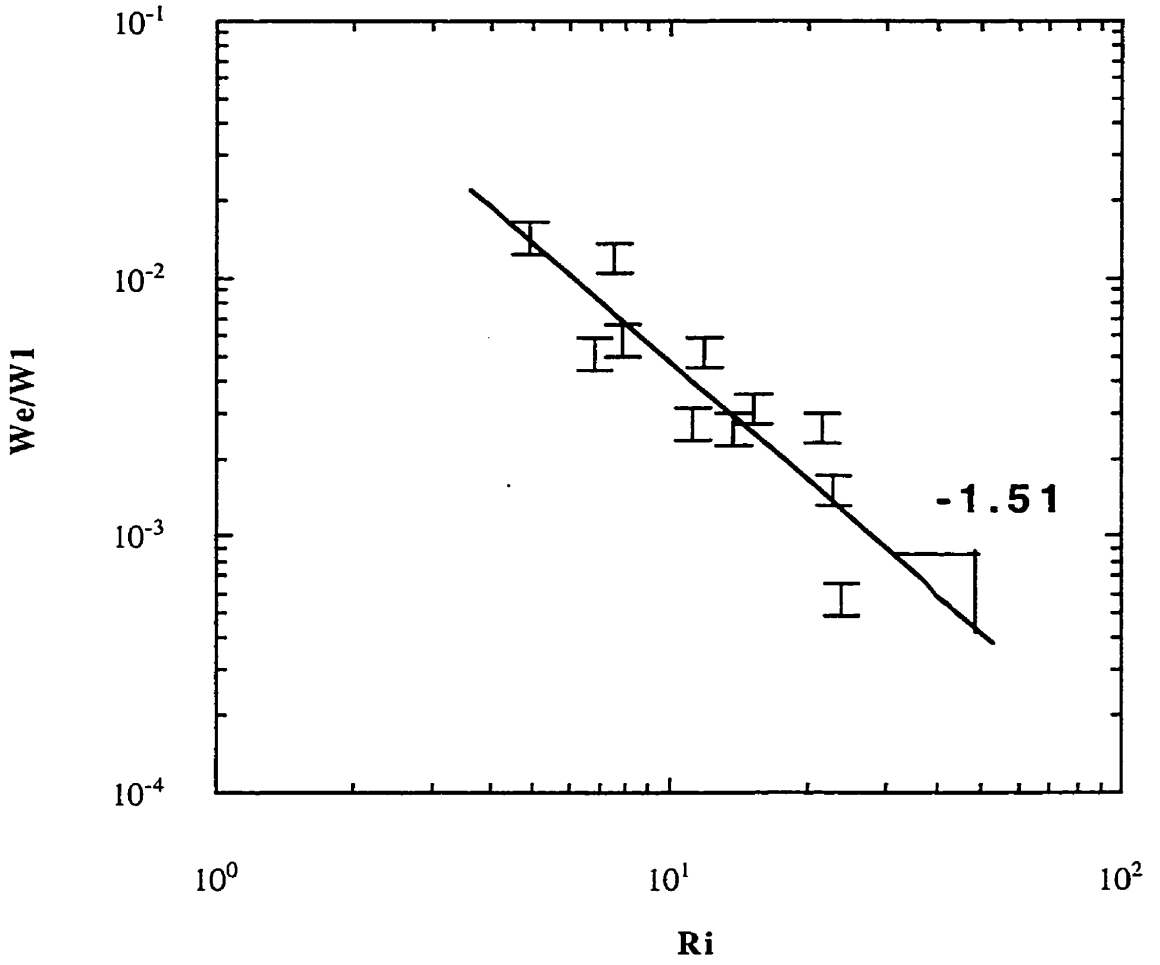

Figure 6a. Entrainment rate (w_e/w_l) vs. Richardson number (Ri) for the classical thermal case 1

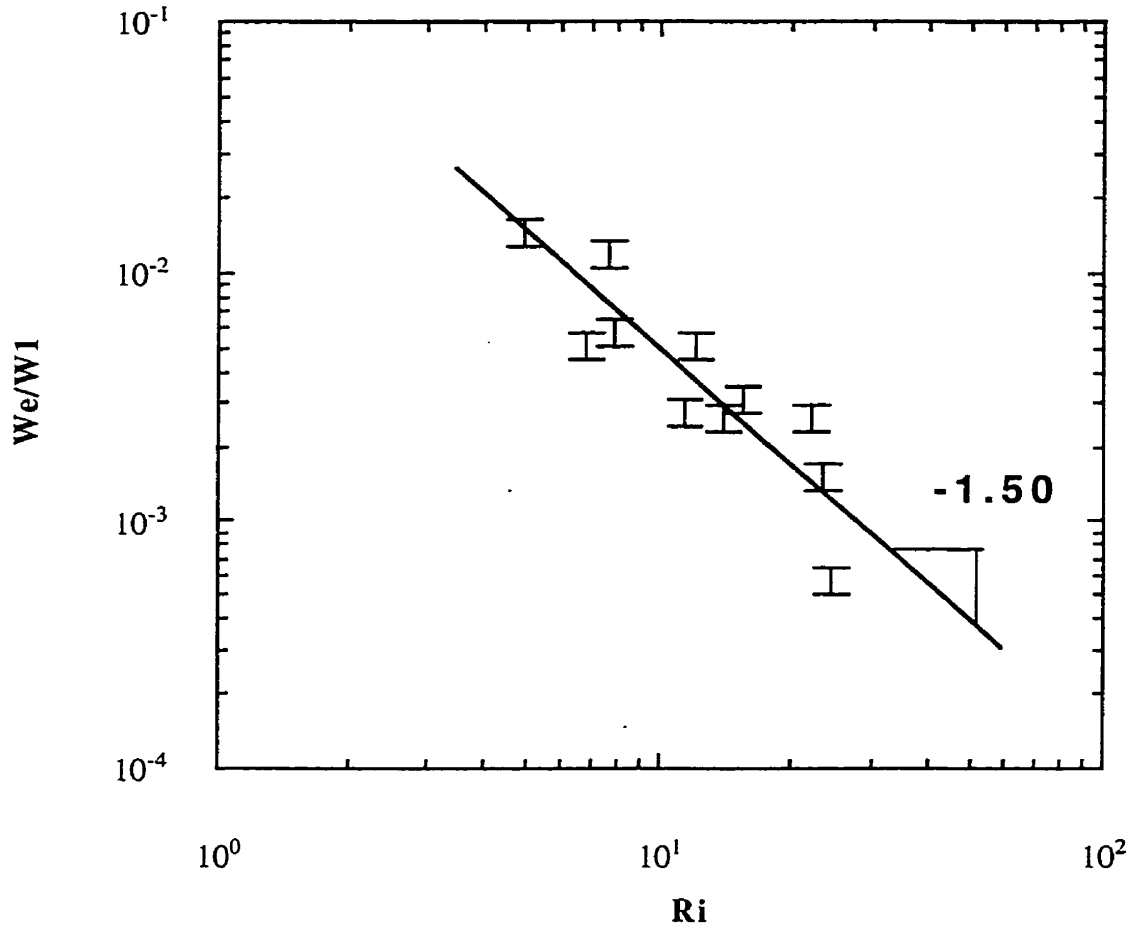

Figure 6b. Entrainment rate (w_e/w_1) vs. Richardson number (Ri) for the classical thermal case 2

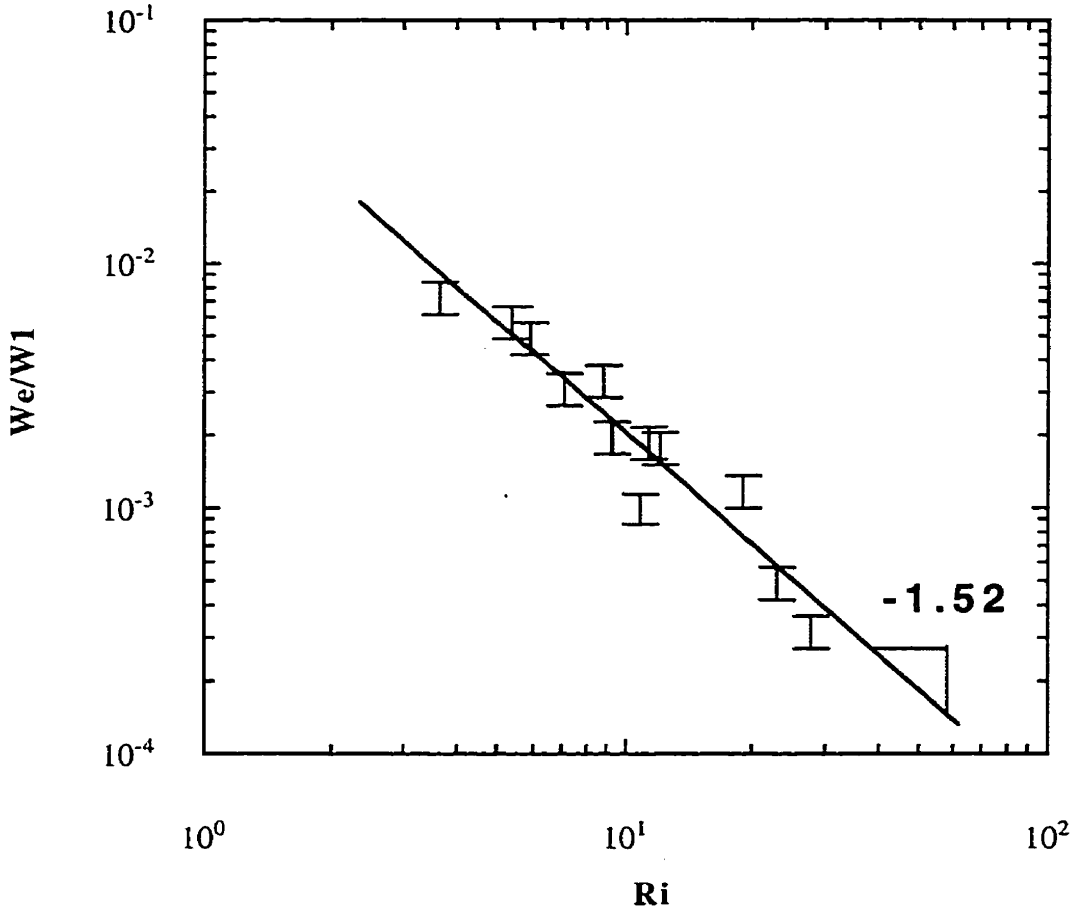

Figure 6c. Entrainment rate (w_{e/w_1}) vs. Richardson number (Ri) for the classical thermal case 3

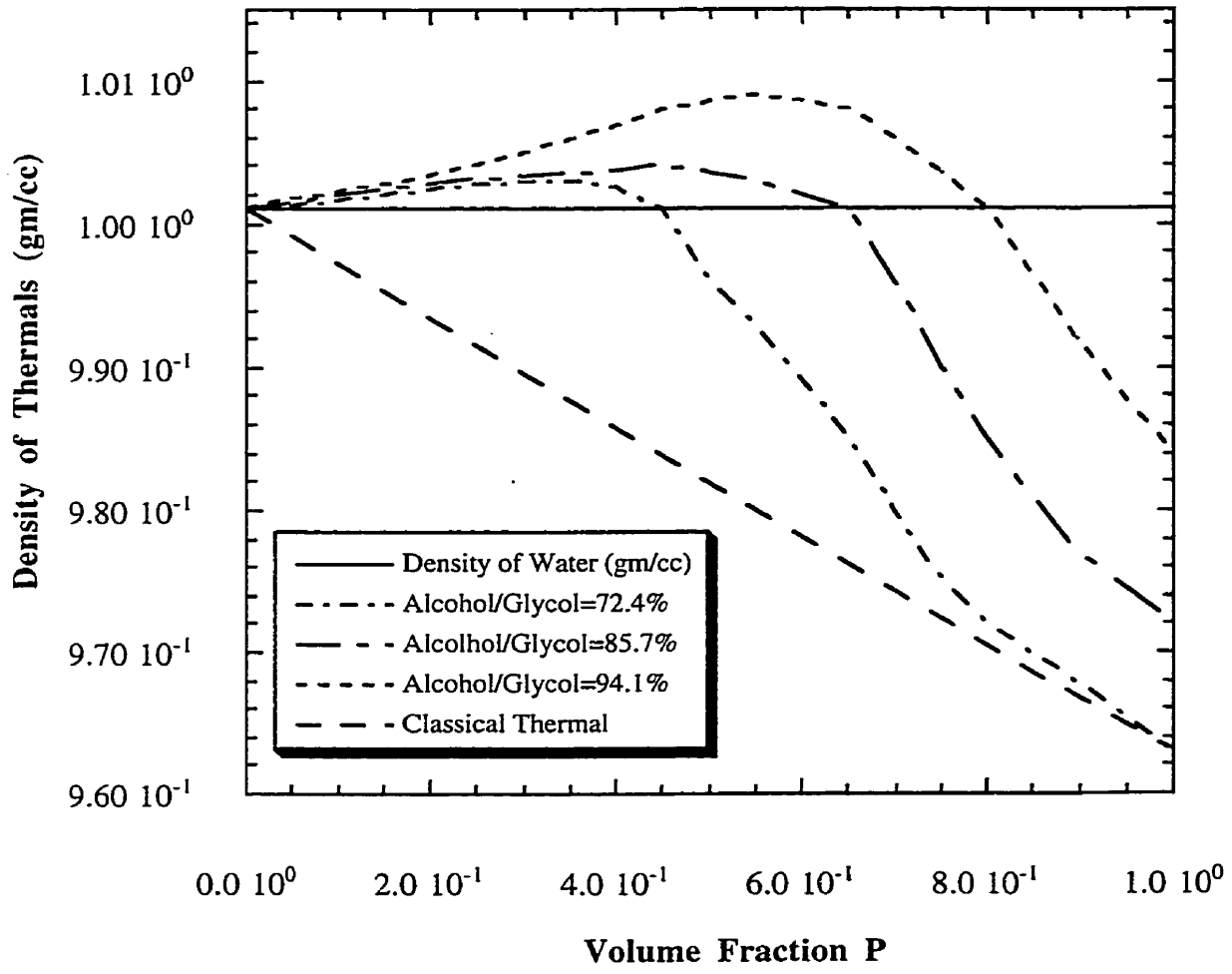

Figure 7. Density ρ as a function of volume fraction P

Figure 8a. Photograph of a thermal with buoyancy reversal (D*=0.16) just after release

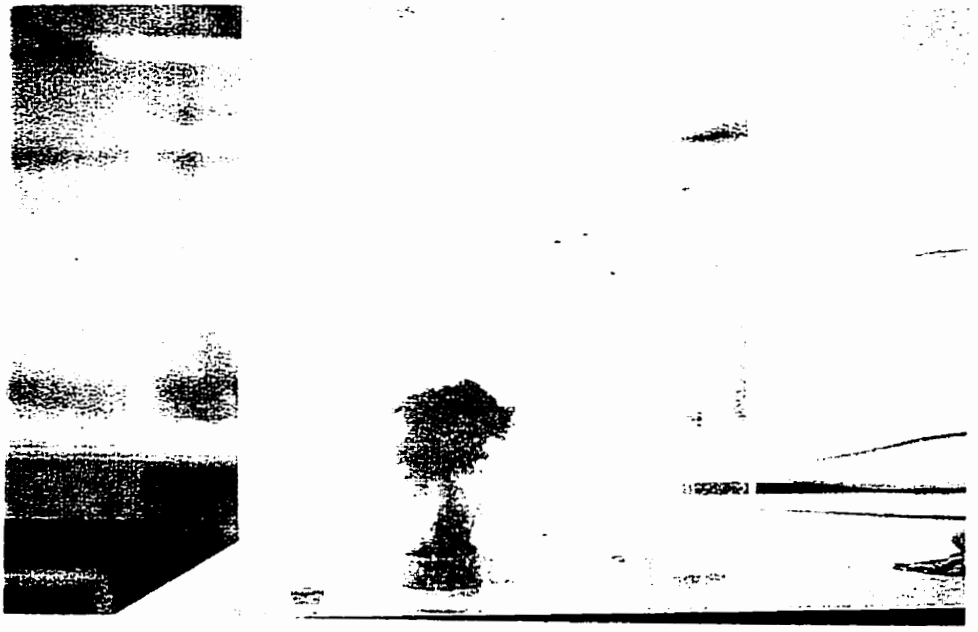

Figure 8b. Photograph of a thermal with buoyancy reversal (D*=0.16) before impinging on the stratified interface

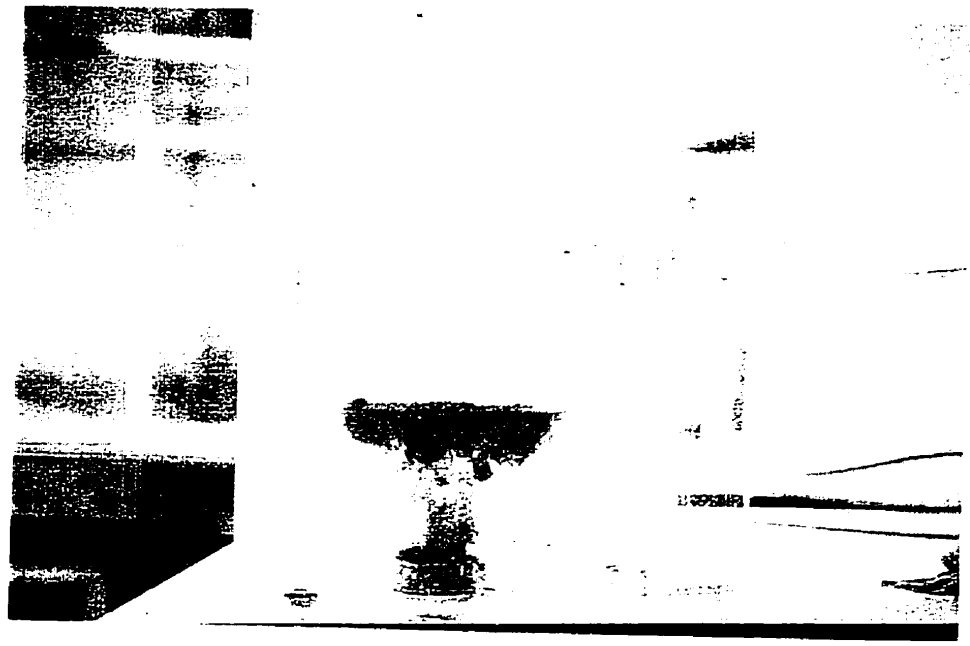

Figure 8c. Photograph of a thermal with buoyancy reversal (D*=0.16) impinging on the stratified interface

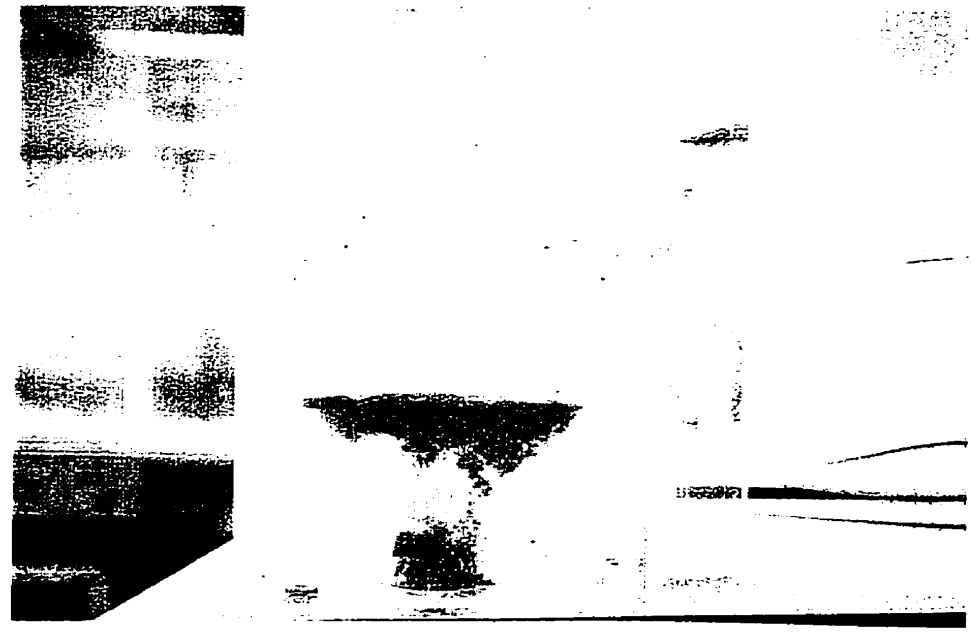

Figure 8d. Photograph of a thermal with buoyancy reversal (D*=0.16) after impingement on the stratified interface

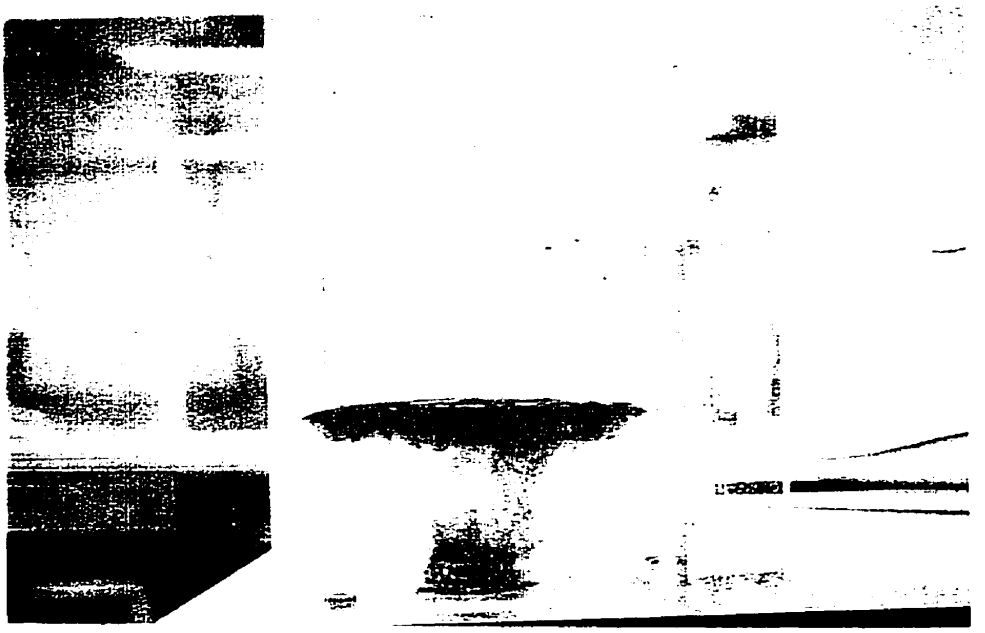

Figure 8e. Photograph of a thermal with buoyancy reversal (D*=0.16) collapse after impingement on the stratified interface

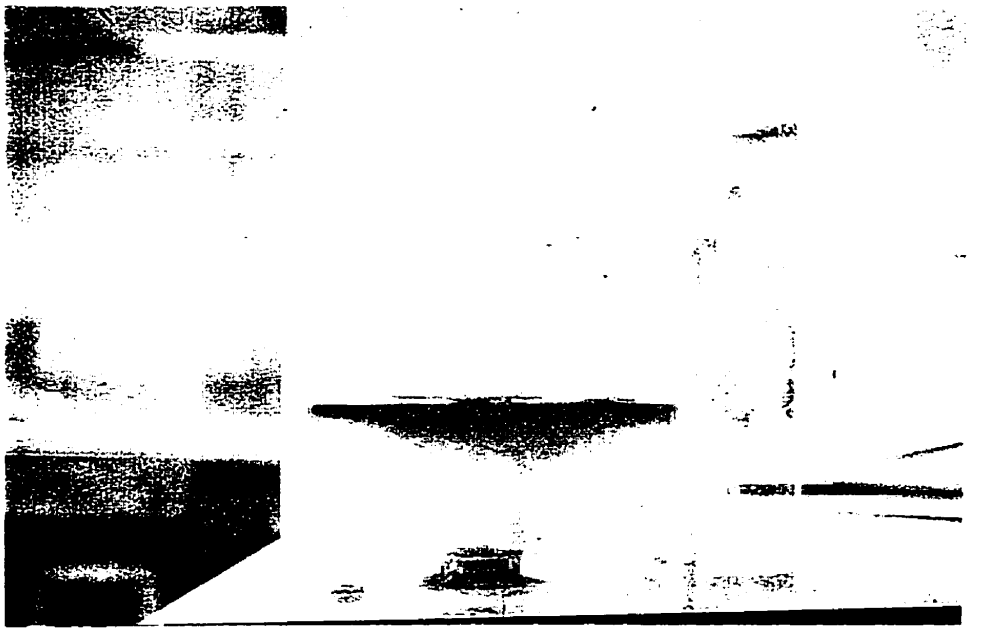

Figure 8f. Photograph of the final stage of a thermal with buoyancy reversal (D*=0.16)

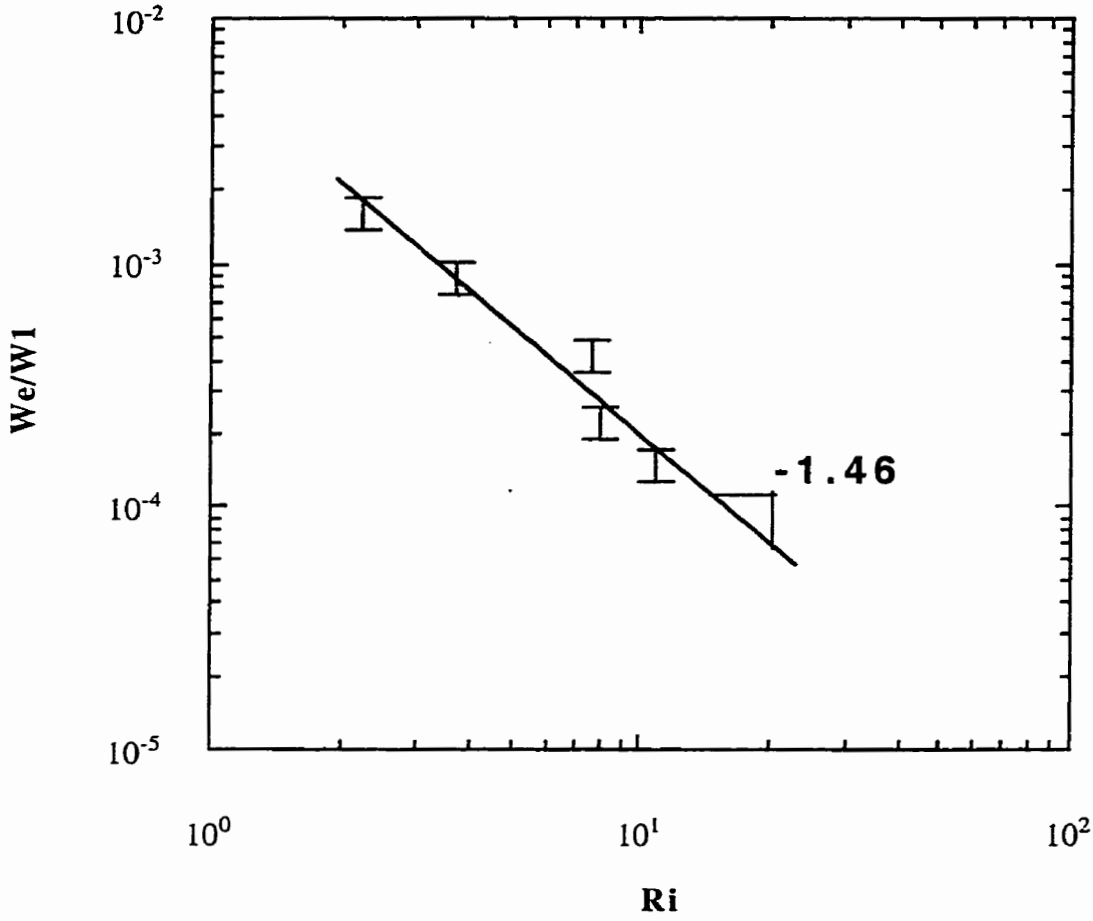

Figure 9a. Entrainment rate (w_e/w_1) vs. Richardson number (Ri) for D*=0.053.

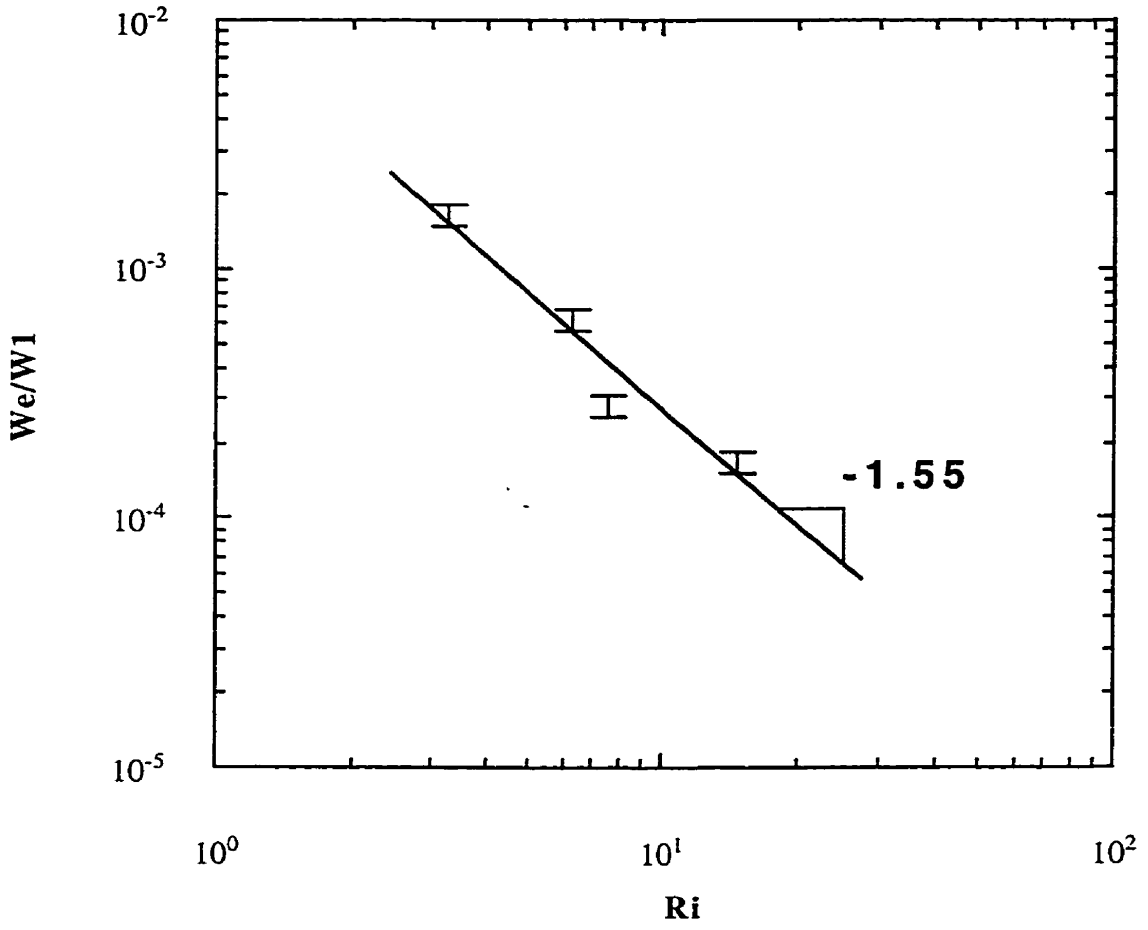

Figure 9b. Entrainment rate (w_e/w_l) vs. Richardson number (Ri) for D*=0.078.

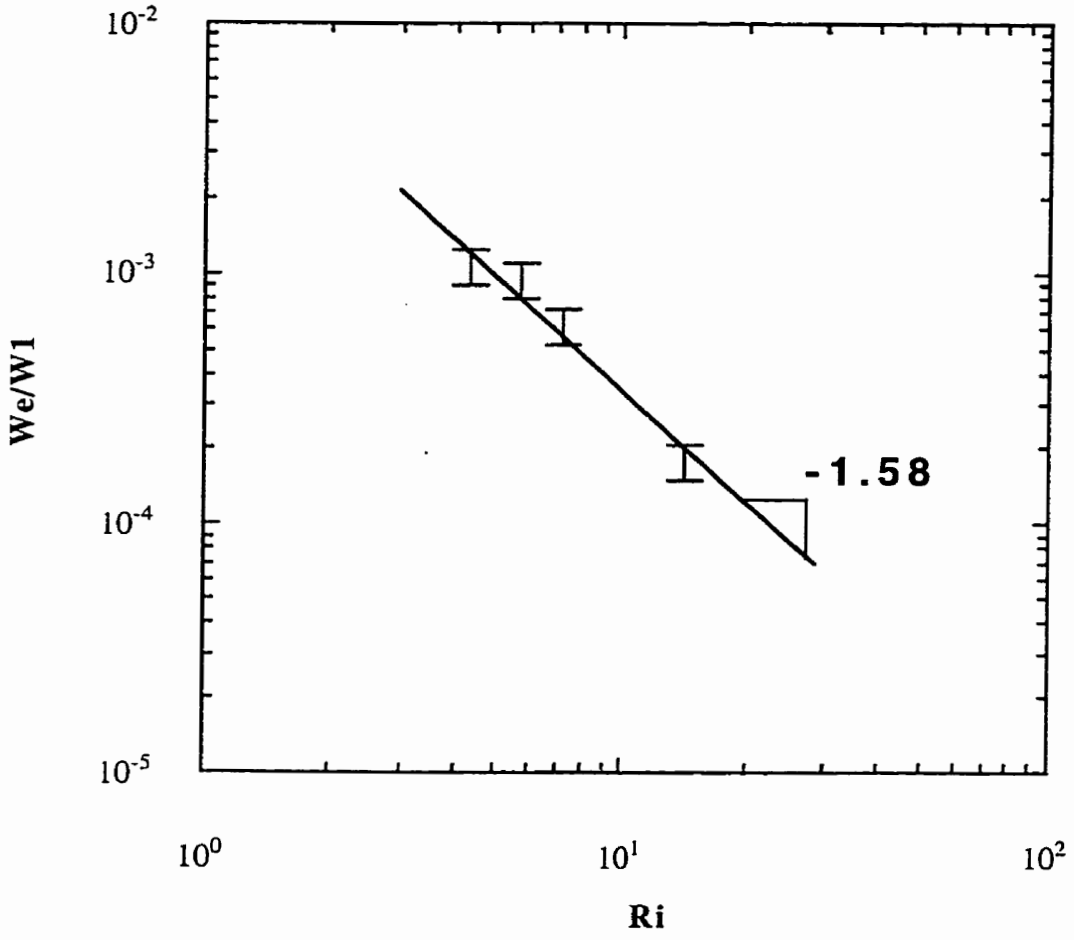

Figure 9c. Entrainment rate (w_e/w_1) vs. Richardson number (Ri) for D*=0.16.

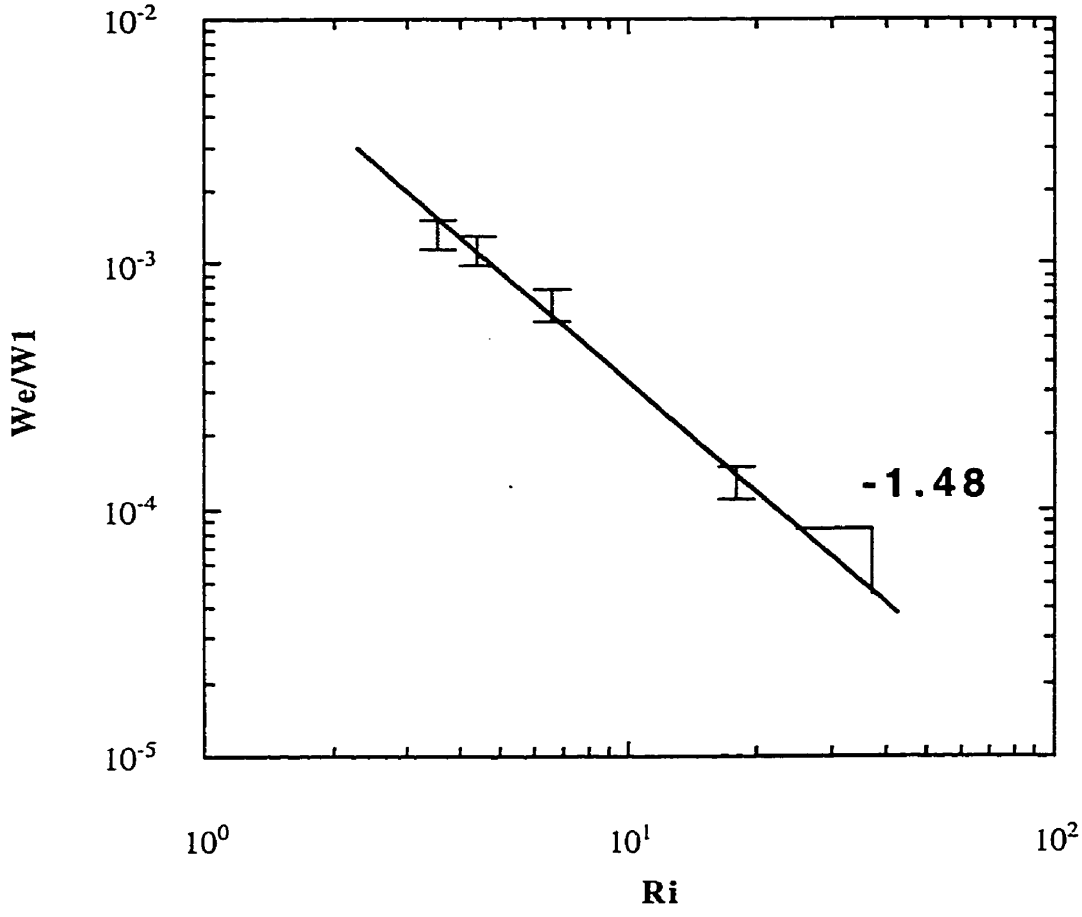

Figure 9d. Entrainment rate (w_e/w_1) vs. Richardson number (Ri) for D*=0.214.

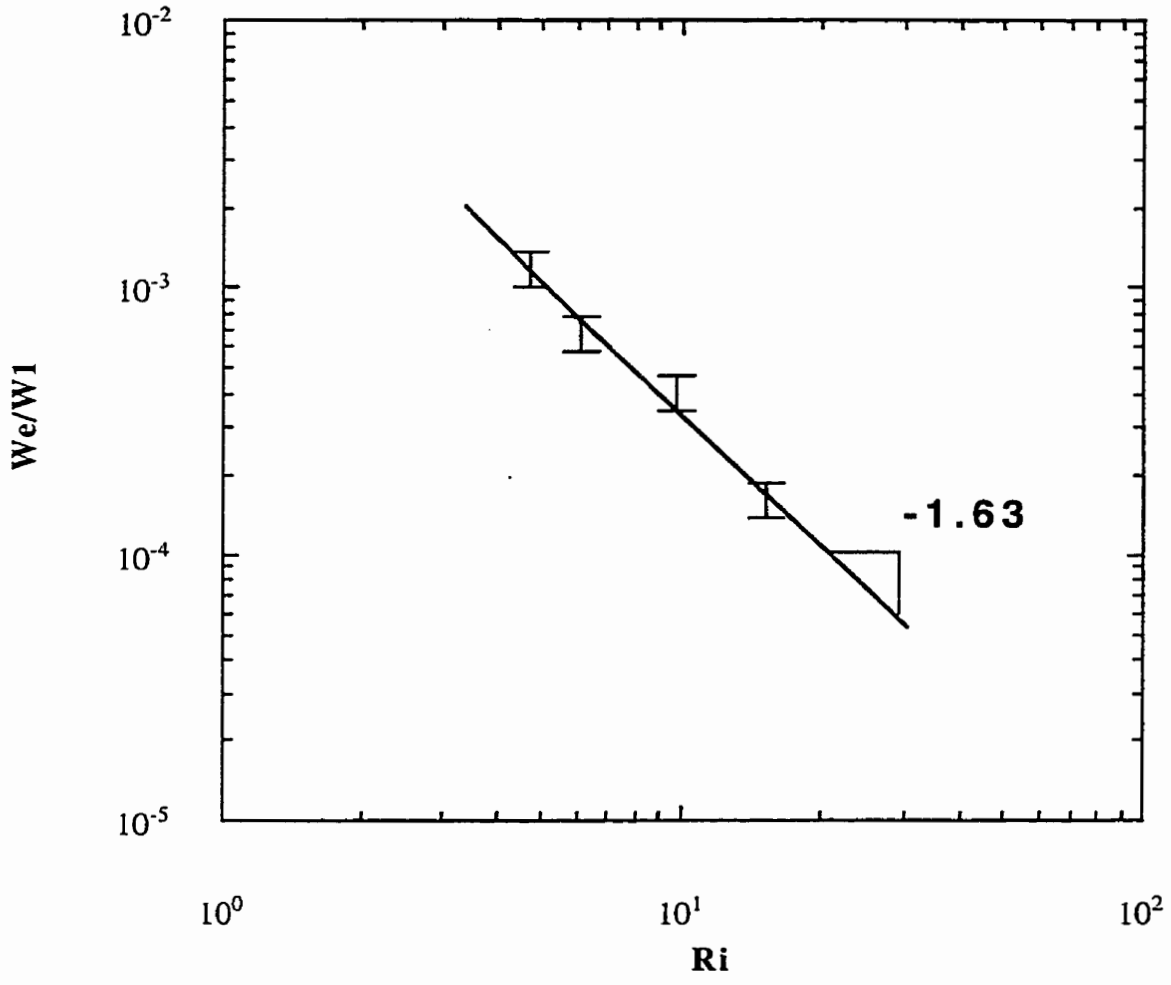

Figure 9e. Entrainment rate (w_e/w_1) vs. Richardson number (Ri) for D*=0.471.

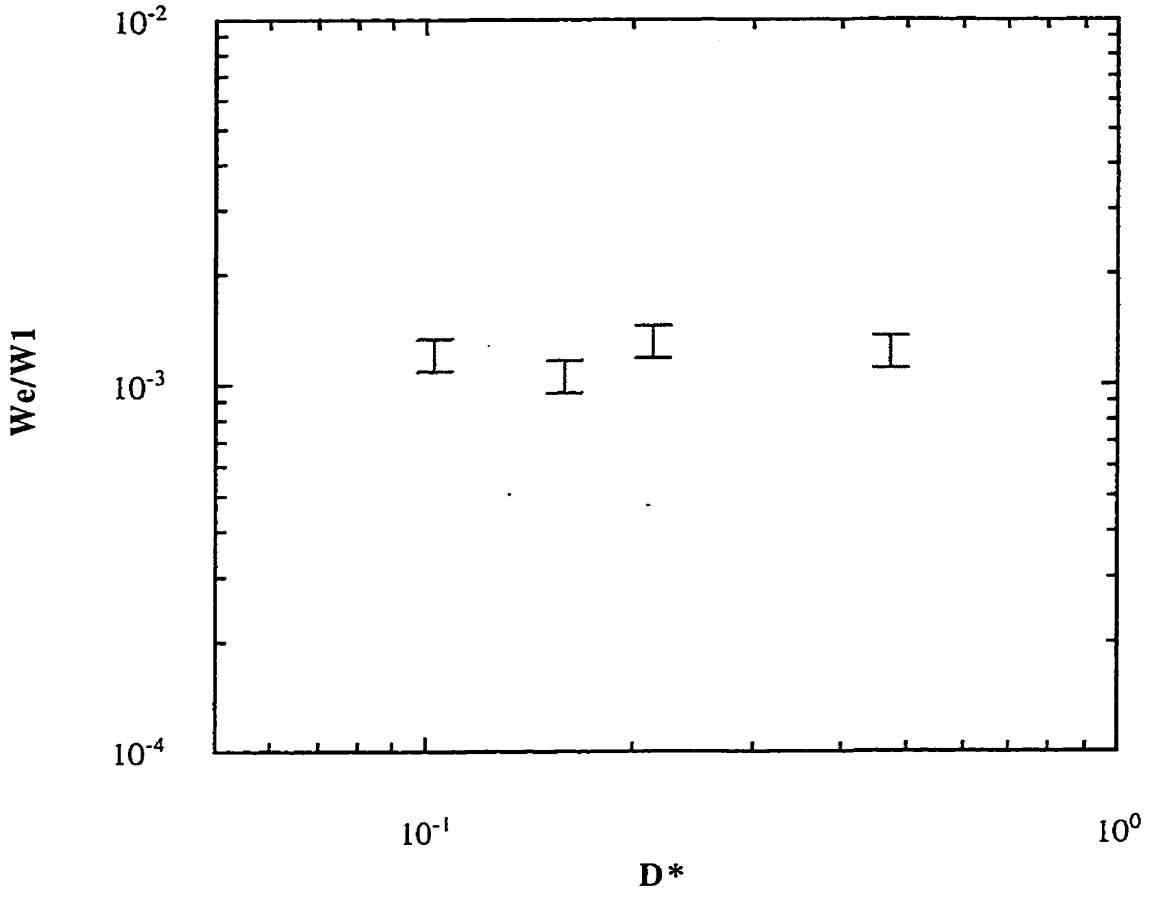

Figure 10a. Entrainment rate (w_e/w_1) vs. Buoyancy reversal parameter (D*) for Ri=4.

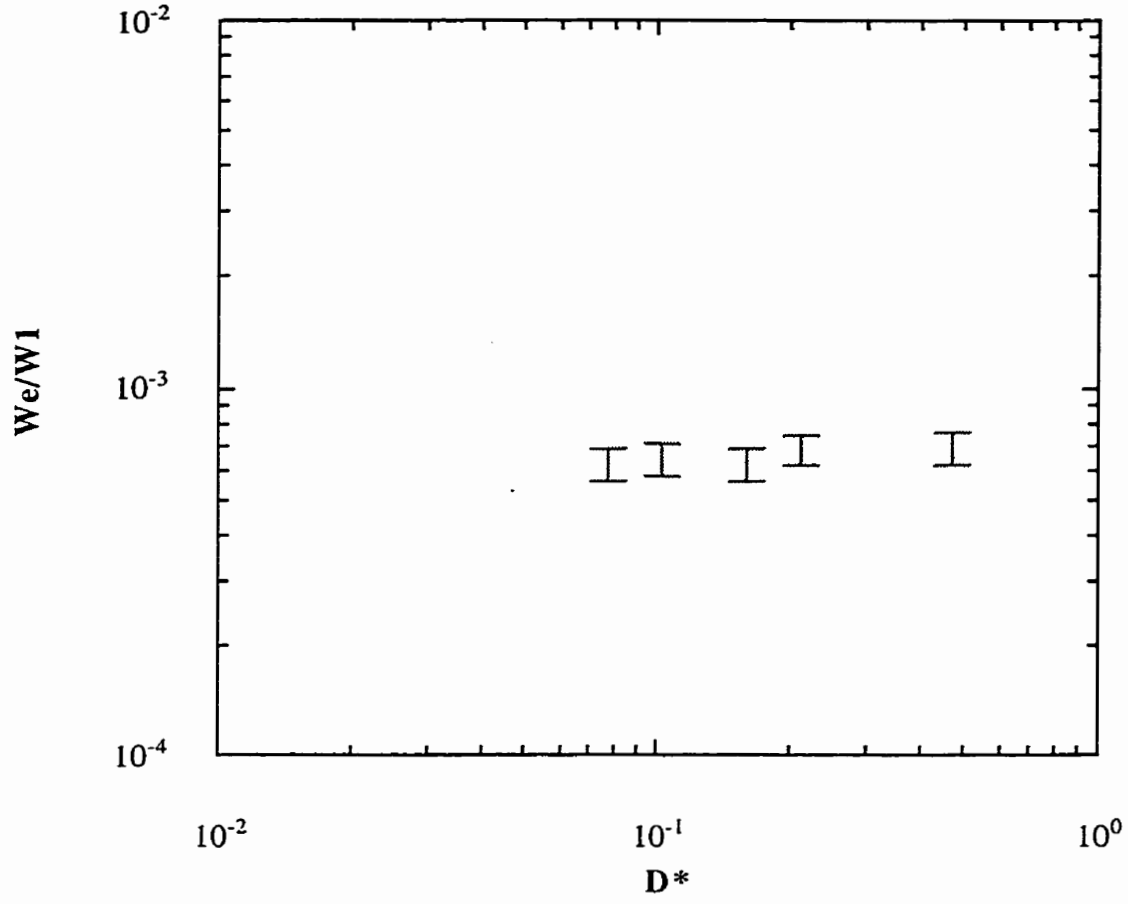

Figure 10b. Entrainment rate (w_e/w_1) vs. Buoyancy reversal parameter (D*) for Ri=6.

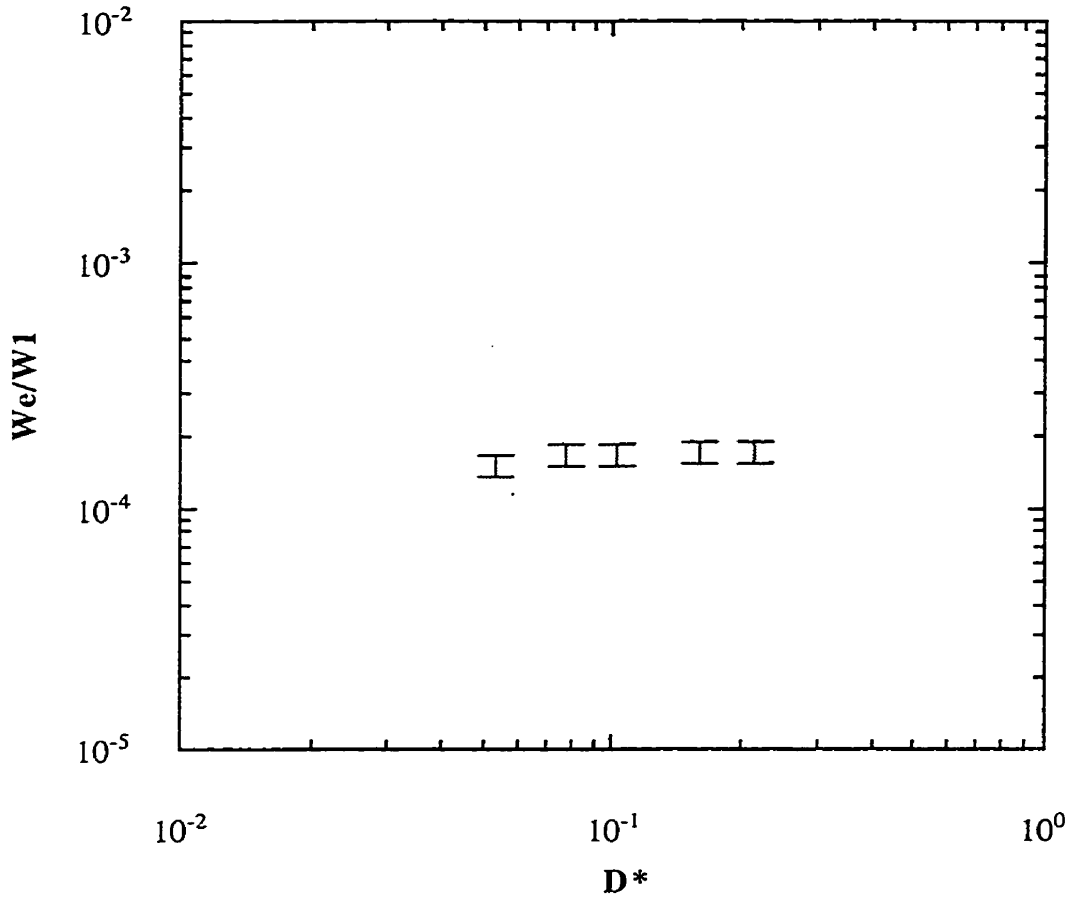

Figure 10c. Entrainment rate (w_e/w_l) vs. Buoyancy reversal parameter (D*) for Ri=10.

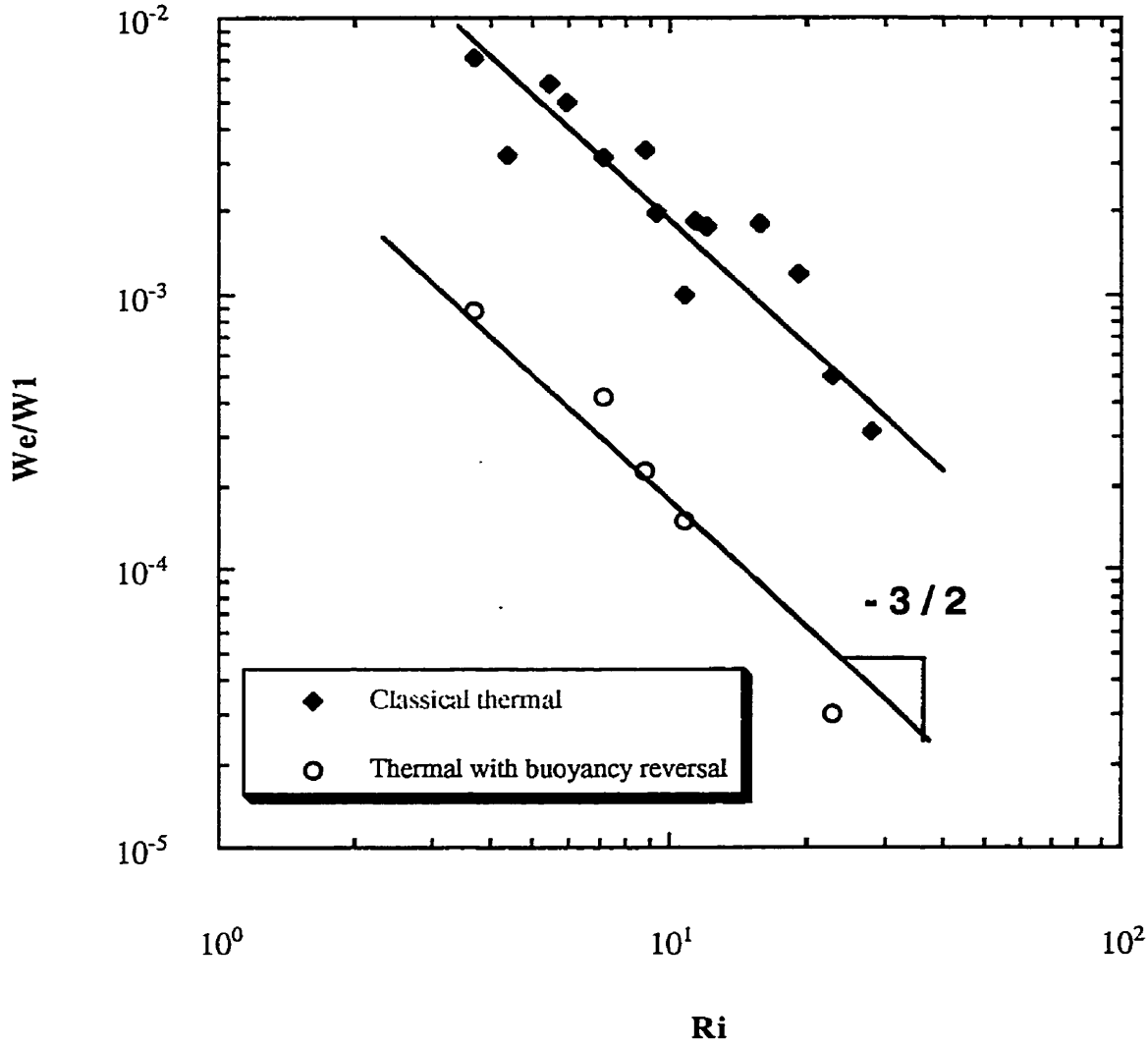

Figure 11. Comparison of the entrainment rate (w_e/w_1) vs. Richardson number (Ri) with and without buoyancy reversal

References

Batchelor, G. K. (1954) - Heat convection and buoyancy effects in fluids, *Quart. J. Met. Soc.*, **80**, 339-358.

Betts, A. K. (1973) - Non-precipitating cumulus convection and its parameterization, *Quart. J. Roy. Met. Soc.*, **99**, 178-196.

Blyth, A. M., Cooper, W. A. and Jensen, J. B. (1988) - A study of the source of entrained air in Montana cumuli, *J. Atmos. Sci.*, **45**, 3944-3964.

Breidenthal, R. E. and Baker, M. B. (1985) - Convection and entrainment across stratified interfaces, *J. Geophy. Research*, **90**, No. D7, 13,055-13,062.

Bretherton, C. S. and Smolarkiewicz, P. K. (1989) - Gravity waves compensating subsidence and detrainment around cumulus clouds, *J. Atmos. Sci.*, **46**, 740-759.

Caughey, S. J. and Palmer, S. G. (1979) - Some aspects of turbulence structure through the depth of the convective boundary layer, *Quart. J. Roy. Met. Soc.*, **105**, 811-827.

Cotel, A. J. (1995) - Entrainment and detrainment of a jet impinging on a stratified interface, Ph. D. Thesis, University of Washington, Department of Aeronautics and Astronautics.

Cotel, A. J. and Breidenthal, R. E. (1997) - A model of stratified entrainment using vortex persistence, *Applied Scientific Research*, **57**, 349-366.

Cotel, A. J., Gjestvang, J. A., Ramkhelawan, N. N., and Breidenthal, R. E. (1997) - Laboratory experiments of a jet impinging on a stratified interface, *Experiments in Fluids*, **23**, 155-160.

Dai, Z., Tseng, L. K. and Faeth, G. M. (1994) - Structure of round, fully-developed, buoyant turbulent plumes, *J. Fluid Mech.*, **116**, 409-417.

Deardorff, J. W. (1980) - Cloud-top entrainment instability, *J. Atmos. Sci.*, **37**, 131-147.

Grabowski, W. W. and Clark, T. L. (1991) - Cloud-environment interface instability: Rising thermal calculations in two spatial dimensions, *J. Atmos. Sci.*, **48**, 527-546.

Grabowski, W. W. and Clark, T. L. (1993) - Cloud-environment interface instability. Part II: Extension to three spatial dimensions, *J. Atmos. Sci.*, **50**, No. 4, 555-573.

Grabowski, W. W. (1995) - Entrainment and mixing in buoyancy-reversing convection with applications to cloud-top entrainment instability, *Quart. J. Roy. Met. Soc.*, **121**, No. 522, 231-253.

Hu, Q. (1998) - A cumulus parameterization based on a cloud model of intermittently rising thermals, *J. Atmos. Sci.*, **54**, 2292-2307.

Johari, H. (1989) - An experimental investigation of mixing in buoyant flows, Ph. D. Thesis, University of Washington, Department of Aeronautics and Astronautics.

Johari, H. (1992) - Mixing in thermals with and without buoyancy reversal, *J. Atmos. Sci.*, **50**, No. 16, 1412-1426.

Kumagai, M. (1984) - Turbulent buoyant convection from a source in a confined two-layered region, *J. Fluid Mech.*, **147**, 105-131.

Linden, P. F. (1973) - The interaction of a vortex ring with a sharp density interface: a model for turbulence entrainment, *J. Fluid Mech.*, **60**, 467-480.

Randall, D. S. (1980) - Conditional instability of the first kind upside-down, *J. Atmos. Sci.*, **37**, 125-130.

Richards, J. M. (1962) - Experiments on the penetration of an interface by buoyant thermals, *J. Fluid Mech.*, **11**, 369-384.

Roshko, A. (1976) - Turbulent shear flow: A new look, *AIAA J.*, **14**, 1349-1357.

Saunders, P. M. (1962) - Penetrative convection in stably stratified fluids, *Tellus*, **14**, 177-194.

Scorer, R. S. (1957) - Experiments on convection of isolated masses of buoyant fluid, *J. Fluid Mech.*, **2**, 583-594.

Scorer, R. S. (1958) - Natural Aerodynamics, *Pergamon Press*, London, 312.

Siems, S. T., Christopher, S. B., Baker, M. B., Shy, S. S. and Breidenthal, R. E. (1990) - Buoyancy reversal and cloud-top entrainment instability, *Quart. J. Roy. Met. Soc.*, **116**, 705-739.

Shy, S. S. and Breidenthal, R. E. (1990) - Laboratory experiments on the cloud-top entrainment instability, *J. Fluid Mech.*, **214**, 1-15.

Taylor, G. R. and Baker, M. B. (1991) - Entrainment and detrainment in cumulus clouds, *J. Atmos. Sci.*, **48**, 112-121.

Turner, J. S. (1963) - Model experiments relating to thermals with increasing buoyancy, *Quart. J. Met. Soc.*, **89**, 62-74.

Turner, J. S. and Yang, I. K. (1963) - Turbulent mixing at the top of stratocumulus clouds, *J. Fluid Mech.*, **17**, 212-224.

Turner, J.S. (1964) - The dynamics of spherical masses of buoyant fluid, *J. Fluid Mech.*, 19, 481-490.

Turner, J. S. (1966) - Jets and plumes with negative or reversing buoyancy, *J. Fluid Mech.*, **26**, part 4, 779-792.

Turner, J. S. (1973) - Buoyancy Effects in Fluids, *Cambridge University Press*, 165-206.

Turner, J. S. (1986) - Turbulence entrainment: the development of the entrainment assumption, and its application to geophysical flows, *J. Fluid Mech.*, **173**, 431-471.

Wallace, J. M. and Hobbs, P. V. (1977) - Atmospheric science: An introductory survey, *Academic Press*, INC.

Woodward, B. (1959) - The motion in and around isolated thermals, *Quart. J. Met. Soc.*, **85**, 144-151.

Young, G. S. (1988) - Turbulence structure of the convection boundary layer. Part II: Phoenix 78 aircraft observation of thermals and their environment, *J. Atmos. Sci.*, **45**, No. 4, 727-735.

APPENDIX

TABLE A. Parts of the water tank and release mechanism

Order	Name	Number	Material	Remark
1	Left Wall	1	Lucite Plastic	
2	Front & Back Wall	1	Lucite Plastic	
3	Right Wall < upper / lower	2	Lucite Plastic	
4	Bottom	1	Lucite Plastic	
5	Sealing Lips (1)	2	Lucite Plastic	Including sealing rubber
6	Sealing Lips (2)	2	Lucite Plastic	Including sealing rubber
7	Partition Plate	1	Stainless Steel	
8	Container Lid	1	Stainless Steel	
9	Container	1	PVC Pipe	
10	Plug	1	Lucite Plastic	Including sealing rubber between the bottom wall and the plug

Figure A. Schematic 3-D Drawing

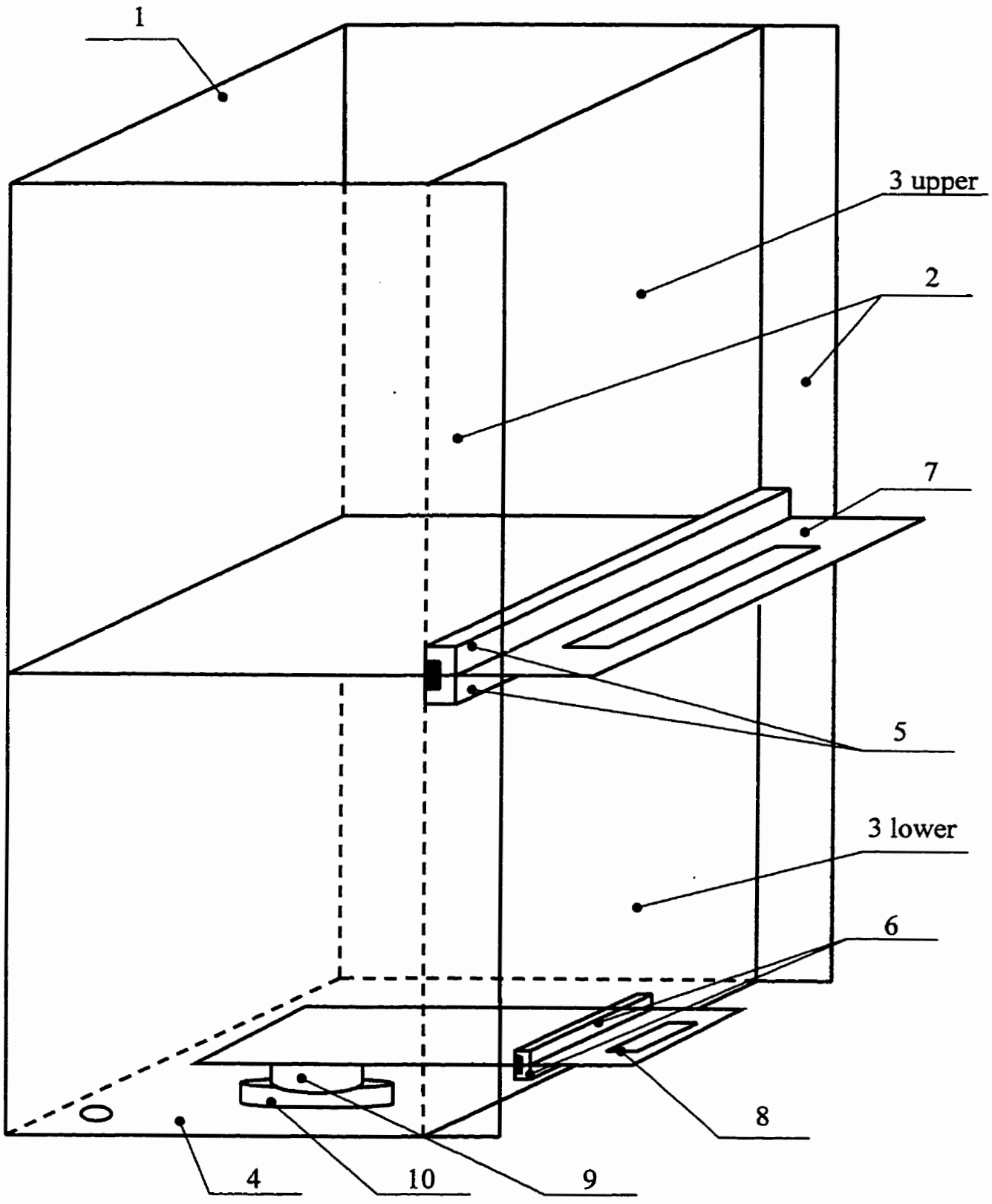

Figure A-1

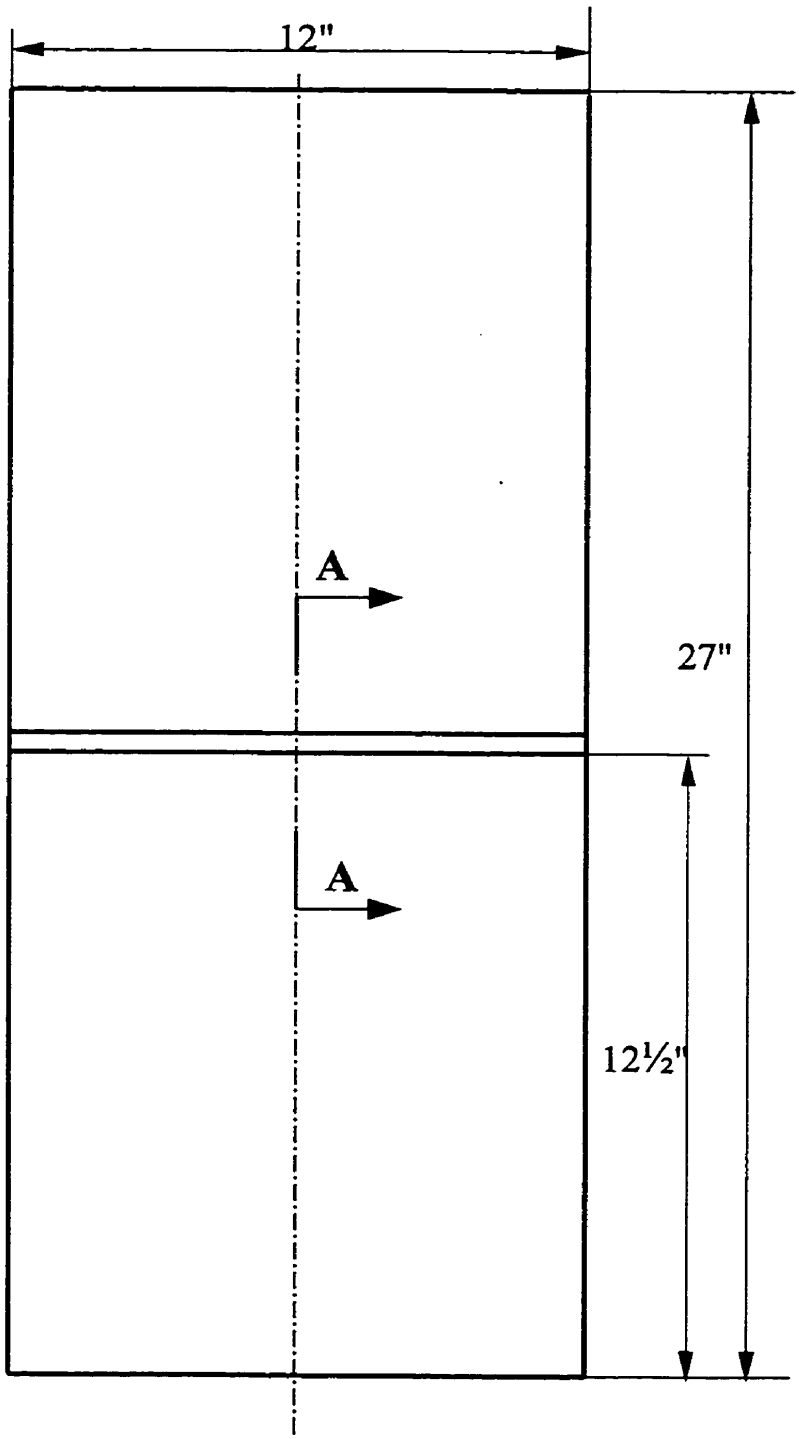

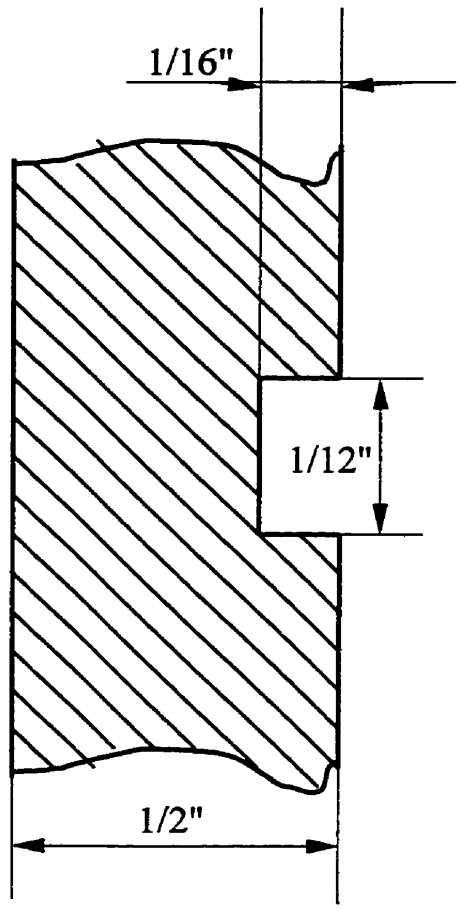

Figure A-2

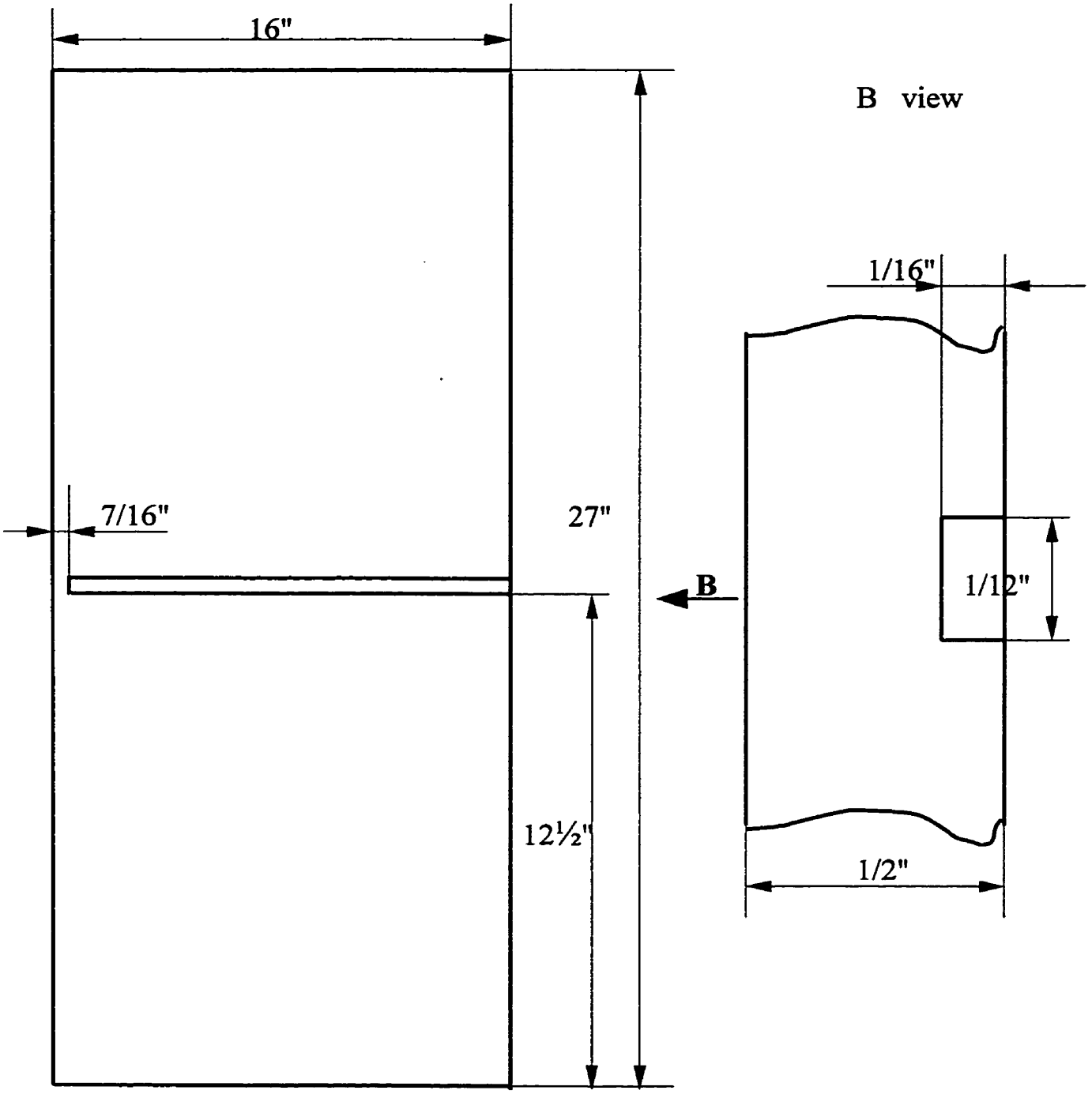

Figure A-3

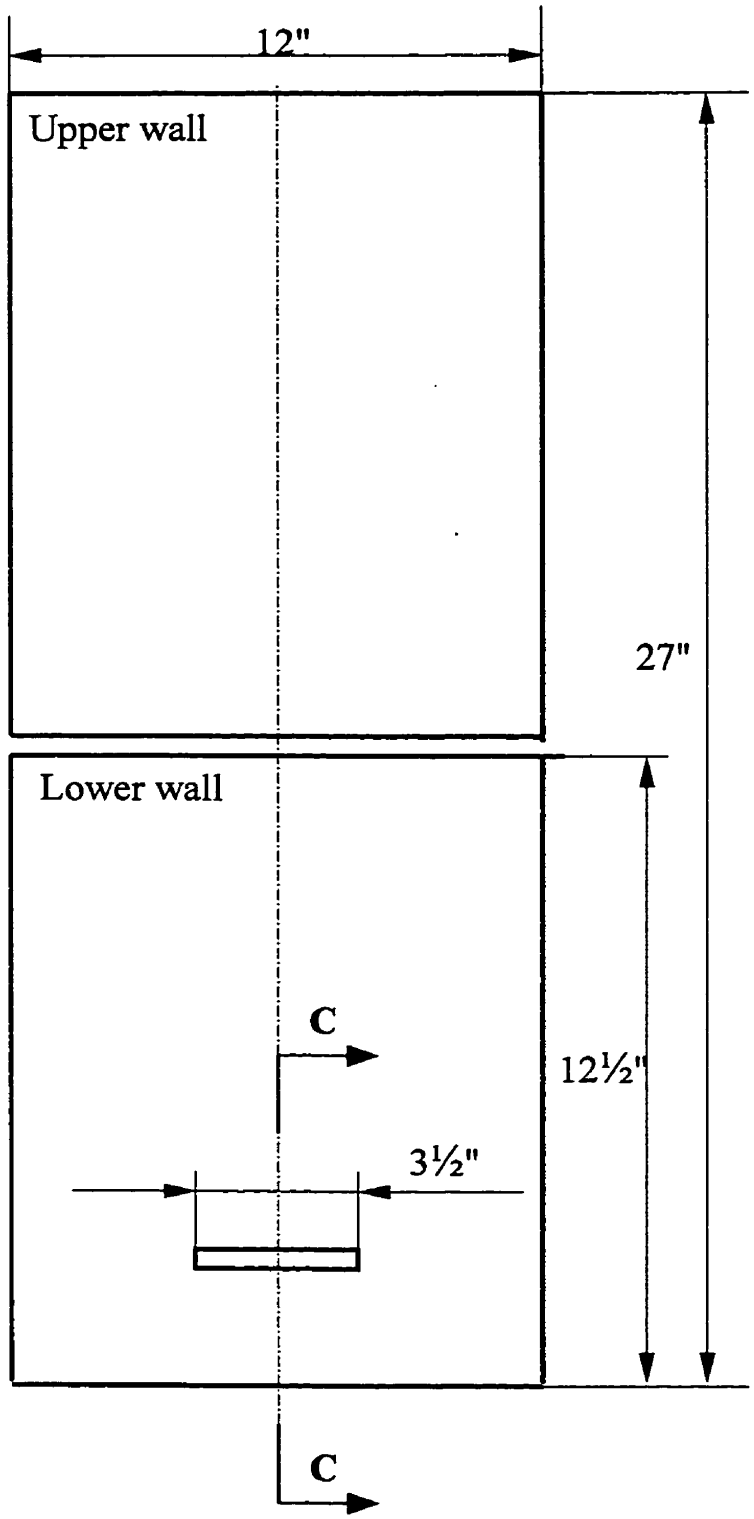

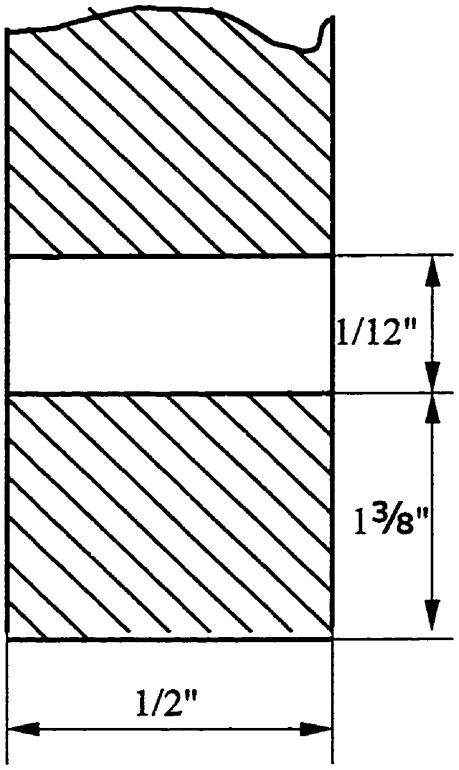

Figure A-4

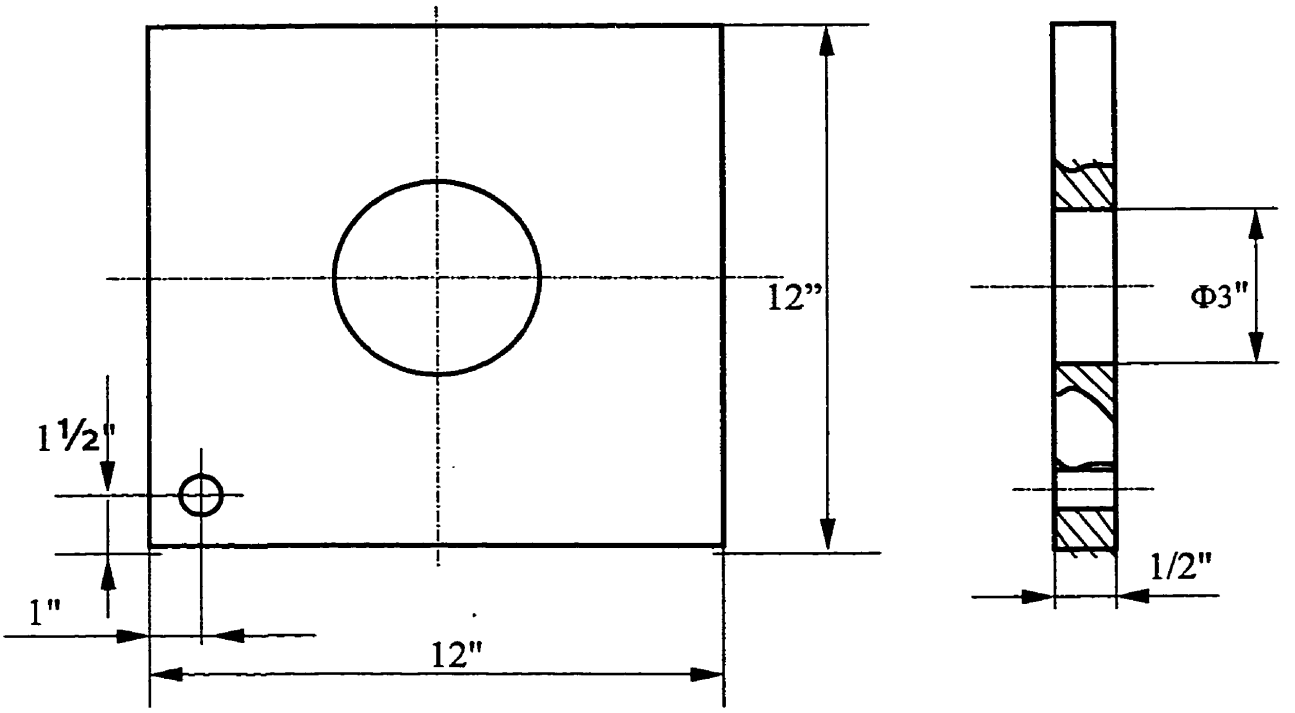

Figure A-5

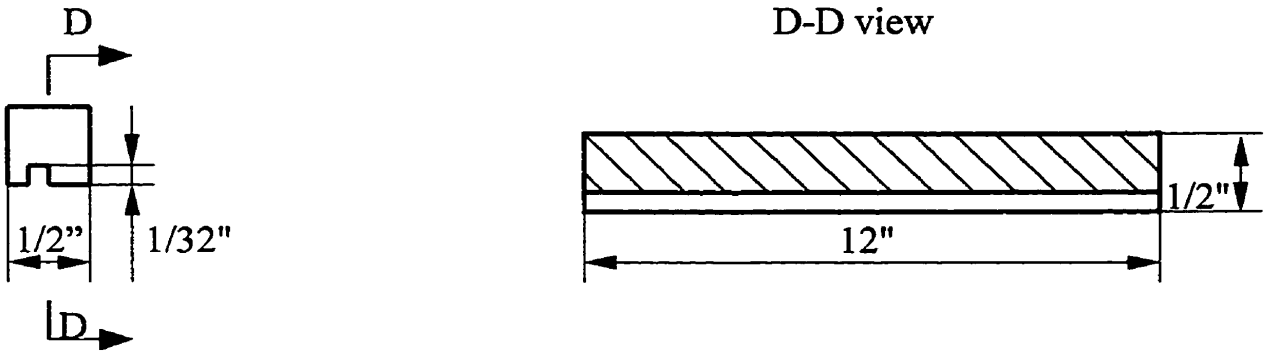

Figure A-6

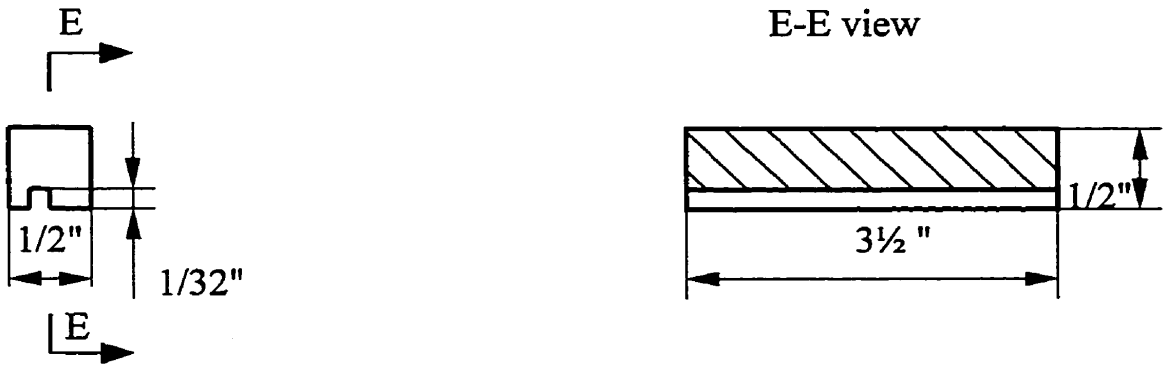

Figure A-7

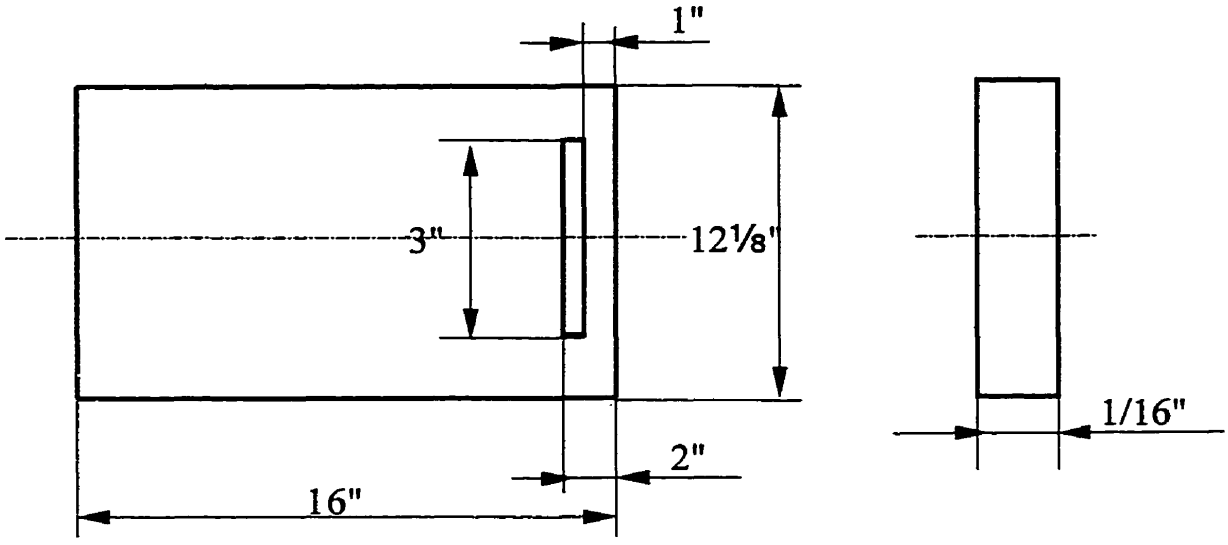

Figure A-8

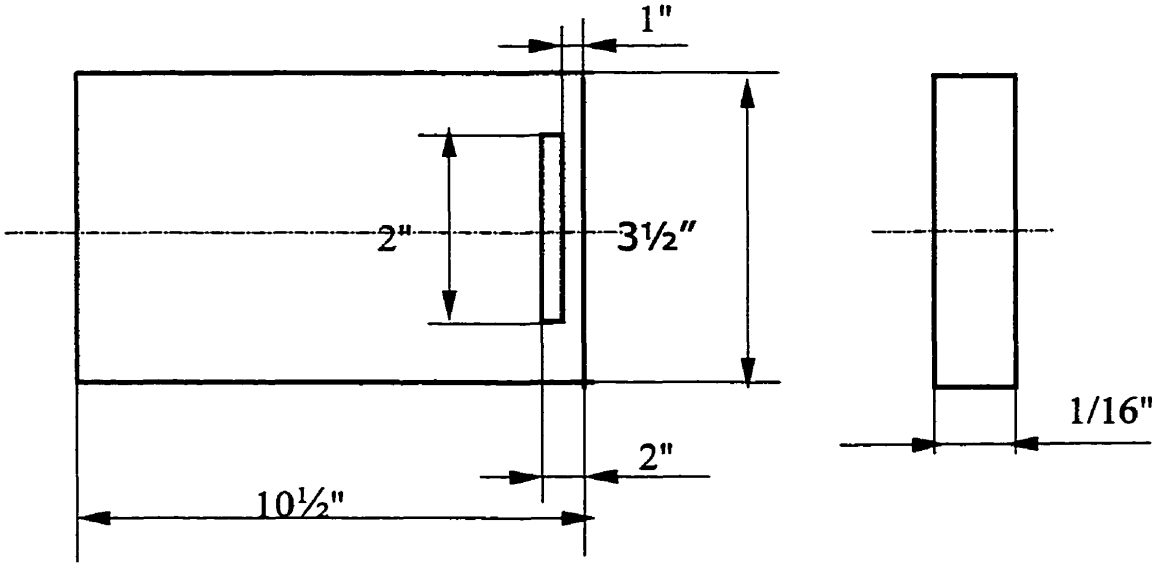

Figure A-9

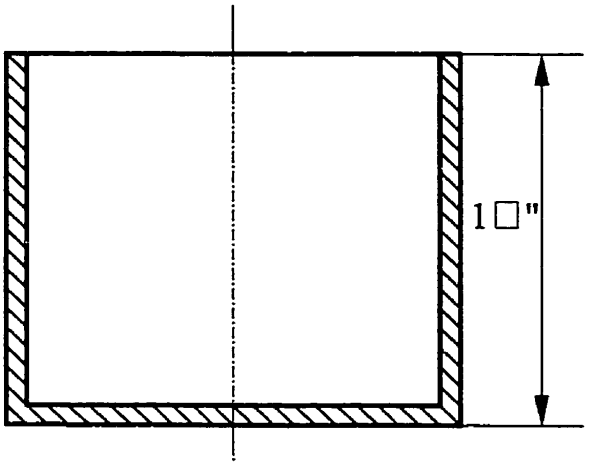

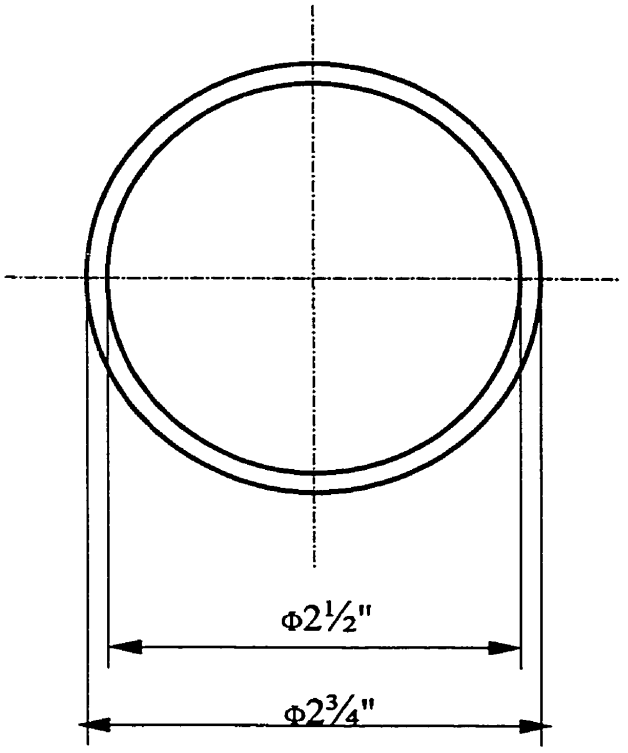

Figure A-10